PEOPLE'S DEMOCRATIC REPUBLIC OF ALGERIA

MINISTRY OF HIGHER EDUCATION AND SCIENTIFIC RESEARCH

AMAR TELIDJI UNIVERSITY- LAGHOUAT

FACULTY OF TECHNOLOGY

Electronic departement

Dissertation Master Degree in Microelectronic Engineering

Presented by: CHAIN MOHAMMED

A NUMERICAL STUDY OF NEW STRUCTURE OF CZTS/SI BASED HETEROJUNCTION

Board of Examiners:

Chairman:	**Pr**	**LIDJICI Hamza**	**UATL**
Examiner:	**MAA**	**HAMDI Abdelwaheb**	**UATL**
Supervisor:	**MCA**	**SELMANE Naceur**	**UATL**
Co-supervisor:	**Pr**	**CHEKNANE Ali**	**UATL**

2022/2023

Dedications

I dedicate this work to:

My mother, sources of tenderness and love, for her support throughout our educational journey.

My father, who have always supported me

My brothers and sisters, whom I love dearly.

My extended family.

My dear friends and teachers.

Everyone who has collaborated, directly or indirectly, in the development of this work.

Appreciation

dear Dr. Naceur SELMANE, kind supervisor

I would like to express my sincere gratitude to you for your invaluable support and guidance throughout my final dissertation. your expertise and patience have greatly contributed to the success of my work.

I also wish to extend my gratitude to the members of the jury for their thorough evaluation of my project, as well as to my friends for their continuous support.

I would like to thank all those who have contributed, directly or indirectly, to the completion of this dissertation. your collaboration and advice have been highly appreciated.

thank you once again for your invaluable assistance.

Kind regards

Mohamed chain

Figures list

Tables list

List of symbols and abbreviations

H	**Planck's constant**
C	**the speed of light**
$E=hv$	**Photon energy**
H	**Planck constant**
I	**Incident intensity.**
A	**[cm^{-1}] absorption coefficient.**
X	**[cm] penetration depth.**
I_s	**the saturation current.**
A	**the charge of the electron.**
K	**Boltzmann's constant.**
T	**the temperature**
N	**the diode's ideality factor.**
V	**the polarization potential (V)**
J_{CC} ou J_{SC}	**Short-circuit current density.**
V_{CO} ou V_{OC}	**Open circuit voltage.**
FF	**The form factor FF.**
P_{in}	**incident light energy.**
P_{max}	**the maximum energy delivered by the cell.**
IQE	**Quantum efficiency (yield).**
Nph	**Photon flux**
I_D	**Reverse diode current.**
I_0	**Temperature-dependent diode saturation current**
I_{ph}	**Photocurrent, depending on the intensity of irradiation**
γ	**Radiation frequency**
Λ	**Radiation wavelength in µm**
R_{SH}	**Parallel resistance**
R_s	**Series resistance**
V_{pv}	**Cell terminal voltage**
I_{pv}	**Current supplied by the cell**
M	**Material index**
K	**Boltzmann constant**

T	**Temperature in Kelvin**
Q	**Electron charge**
PCE	**Power conversion efficiency.**
HTL	**Material for transporting holes.**
ETL	**Electron transport material.**
Nt	**Defect density.**
ND	**Doping concentration (donor).**
Isc	**Short-circuit current.**
Voc	**Open circuit voltage.**
FF	**Form factor**
H	**Solar cell conversion efficiency.**
SCAPS	**Capacitance Simulator one Dimension Plumb.**
TiO2	**Copper oxide.**
PV	**Photovoltaics.**
PSC	**Power conversion efficiency**
Pm	**Maximum power.**
QE	**Quantum efficiency of the cell.**
Rs	**The series resistance.**
Rp	**shunt resistance**
Iph	**Photocurrent.**
CaTiO3	**Calcium titanate.**
ABX3	**Structure of a generic perovskite crystal.**
LD	**diffusion length**
D	**Diffusion coefficient**
T	**the life of a carrier**
m*	**Affective mass**
Au	**gold**
Al	**Aluminum**
Ag	**Silver**
V	**the potential**
Q	**the elementary charge**
E	**permittivity**
N	**the density of free electrons**
P	**the density of free holes**

ND	**the donor doping density**
NA	**the acceptor doping density**
Pt	**the density of hole traps**
Nt	**the density of electron traps**
Ge	**the optical electron generation rate**
Gh	**the optical hole generation rate**
Re	**the electron recombination rate**
Rh	**the rate of hole recombination.**
Jn	**the electron current density**
Jp	**the current density of the holes**
μ_e	**electron mobility.**
λp	**the mobility of the holes.**
De	**the electron diffusion coefficient.**
Dh	**the diffusion coefficient of the holes**
K	**Boltzmann's constant.**
T	**temperature.**
Le	**the electron's diffusion length.**
Lh	**hole diffusion length.**
τ_e	**the lifetime of the electron**
τ_h	**hole life time**
NC	**the effective density of state of the conduction band**
NV	**the effective density of state of the valence band**
SRH	**Shockley-Read-Hall**
Γ	**the recombination coefficient**
Ni	**intrinsic concentration.**
n0	**the concentration of electrons at equilibrium.**
p0	**the concentration of holes at equilibrium.**
A	**absorption coefficient**
Φm	**exit work**
X	**electronic affinity**
Jph	**the current density generated by the light**
J0	**the saturation current in the dark.**
Eg	**Gap energy.**
MASnI3	**Methylammonium tin tri-iodide**

PEDOT:PSS	**poly(3,4-ethylenedioxythiophene) polystyrene sulphonate**

Contents

GENERAL INTRODUCTION

General introduction

With the sun radiating abundant clean, renewable, and sustainable energy, harnessing this energy in a cost-effective and low-cost manner is enticing and challenging for humanity. Solar energy involves harnessing the well-known phenomenon called the Photovoltaic (PV) effect, in which light is directly converted into electricity.

Among the materials that have attracted significant attention, perovskites are currently expanding due to their technological importance and promising physical properties when applied in photovoltaics. Perovskite can be deposited from a solution, enabling the production of large-area photovoltaic cells. The commercialization of perovskite cells relies on improving installation costs compared to silicon and organic technologies by using light-absorbing materials and electrode materials deposited using low-temperature techniques such as sputtering, printing, roll-to-roll, and spin coating. Perovskites exhibit a high absorption coefficient, high carrier mobility, and long carrier diffusion length. Recent advancements in perovskite-based solar cells have led to the emergence of a new low-cost, high-efficiency photovoltaic technology that could be a viable competitor to silicon-based solar cells, which have dominated the photovoltaic industry. The structure of a perovskite solar cell typically includes the following layers: transparent conductive oxide (TCO) substrate, blocking layer (BL) of compact metal oxide, electron transport layer (ETL), perovskite layer (PL), hole transport layer (HTL), and back contact [1].

In perovskite-based cells, P-type organic and inorganic semiconductor materials are used as hole transport materials (HTL). Spiro-OMeTAD is used in mesoscopic structures, while PEDOT: PSS is used in inverted architectures. Titanium dioxide (TiO2) is used as the electron transport material (ETL) .

To enhance the performance of a photovoltaic solar cell, it is necessary to predict the optimal parameters that contribute to the design of an efficient cell. The main objective of this thesis is to study. The primary objective of this thesis is to investigate the influence of different layers on the photovoltaic performance of tandem solar cell. by using the SCAPS simulation tool. The aim is to study the effect of various thicknesses, band gaps, and dopings of the bottom

layer on the photovoltaic performance. Subsequently, these results will be combined with those of the top solar cell to conduct a comprehensive and in-depth study.

This thesis is structured as follows:

In the first chapter, we will provide an overview of solar cells, their principle of operation based on a physical phenomenon called the photovoltaic effect. We will also present the evolution of solar cell technology, which has gone through several generations based on the structure and materials used.

The second Chapter will showcase the SCAPS software employed for our simulation study. We will delve into perovskite, examining its fundamental properties, with a focus on $CsPbI_2Br$ along with HTL and ETL. Furthermore, we will explore the properties of CZTS solar cells and discuss CZTS/Si structures.

Chapter three focuses on the study and simulation of both bottom and tandem solar cells. We will present the simulation results and examine the impact of different layers on the performance of solar cells, particularly when combining the top and bottom layers.

Finally, we will conclude this dissertation with a general overview of the results obtained throughout this work.

CHAPTER I

PHOTOVOLTAIC SOLAR CELLS

I.1. Introduction

This chapter provides a comprehensive overview of solar energy and photovoltaic technology, which is widely recognized as one of the most efficient methods for converting solar radiation into electrical energy.The first section delves into the fundamental concept of a solar cell, a device designed to harness sunlight and convert it into usable electrical power. It explains how solar cells work, utilizing the photovoltaic effect to generate an electric current when exposed to sunlight.The subsequent section explores the architecture of a photovoltaic cell, highlighting its key components and their roles in the conversion process. It covers the various layers, such as the semiconductor material and the transparent conducting layers, which work in synergy to efficiently capture and convert sunlight into electricity.Moreover, the chapter examines the characteristic parameters of a photovoltaic cell, shedding light on important metrics like open-circuit voltage, short-circuit current, fill factor, and efficiency. These parameters provide valuable insights into the performance and effectiveness of a solar cell.Moving forward, the discussion touches upon the different generations of solar cells, emphasizing the advancements made over time in terms of materials, manufacturing techniques, and efficiency. It explores the evolution from first-generation silicon-based solar cells to second-generation thin-film technologies and the emerging third-generation devices.Lastly, the chapter concludes by outlining the advantages of utilizing photovoltaic cells as a renewable energy source. It highlights their environmental benefits, such as reducing greenhouse gas emissions and dependence on fossil fuels. Additionally, it discusses the potential for cost savings, energy independence, and the scalability of photovoltaic systems for various applications.In summary, this chapter serves as a comprehensive introduction to solar energy and photovoltaic technology, covering the basic principles, architectural components, characteristic parameters, generational advancements, and advantages associated with the use of photovoltaic cells.

I.2. Solar photovoltaic energy

Photovoltaic solar energy (or photovoltaic energy or PVE) is electrical energy produced from solar.radiation using photovoltaic solar panels or photovoltaic solar power plants. It is said to be renewable because its source (The Sun) is considered to be inexhaustible on a human timescale. At the end of its life, a photovoltaic panel will have produced 20 to 40 times the energy required to manufacture and recycle it[2].

I.2.1. The sun

The sun is a small, magnetically active central star of the solar system. It is almost spherical in shape, a ball of gas and plasma. It has a diameter of about 1,392,684 kilometers, equivalent to 109 times the diameter of the Earth, and a mass of 2 x 1030 kg, equivalent to 330,000 times the mass of the Earth. It represents about 99.86% of the mass of the solar system[3]

I.2.2. solar radiation

Solar radiation is made up from photons with wavelengths ranging from the ultraviolet (0.2 µm) to the far infrared (2.5 µm). We use the term AM for (Air Mass) to characterise the solar spectrum in terms of the emitted energy. The total energy transported by solar radiation over a sun-earth distance is of the order of 1,350W/m² (AM0) in space outside the Earth's atmosphere (Figure 1). When solar radiation passes through the atmosphere, it undergoes attenuation and a modification of its spectrum, as a result of absorption and diffusion phenomena in gases, water and dust. In this way, the ozone layer absorbs part of the light spectrum coming from the sun, and in particular the part of the ultraviolet radiation that is harmful to health. The direct solar radiation received from the ground (at 90° inclination) reaches 1,000 W/m² due to absorption in the atmosphere(AM1). This value changes according to the inclination of the light rays in relation to the ground. The lower the angle of penetration θ, the greater the thickness of the atmosphere through which the rays have to pass, resulting in a significant loss of energy. For example, the direct energy transported by solar radiation reaching the ground at an angle of 48° is around 833 W/m² (AM1.5). To know the total radiation received by the ground, we need to add the diffused radiation. Diffused radiation refers to all the radiation whose path between the sun and the observation point is not geometrically rectilinear and which is scattered or reflected by the

atmosphere or the ground. Taking this into account, we obtain a reference for the global spectrum noted (AM1.5) with a power of 1,000W/m², (Figure 2) corresponding to our latitudes[3]

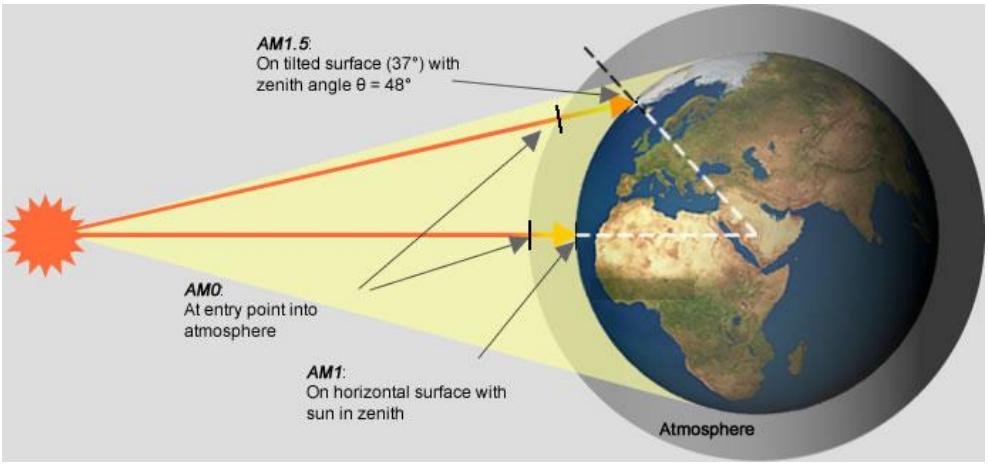

Figure I.1. "Capturing the Sun's Light Energy: Standards for Measuring the Spectrum Concept of the AM convention [4].

The energy of a photon is given by:

$$E = h.\frac{c}{\lambda} \qquad (\mathbf{I.1})$$

Where **h** is Planck's constant, **c** is the speed of light and **λ** is its wavelength. The shorter the wavelength, the greater the energy of the photon [3].

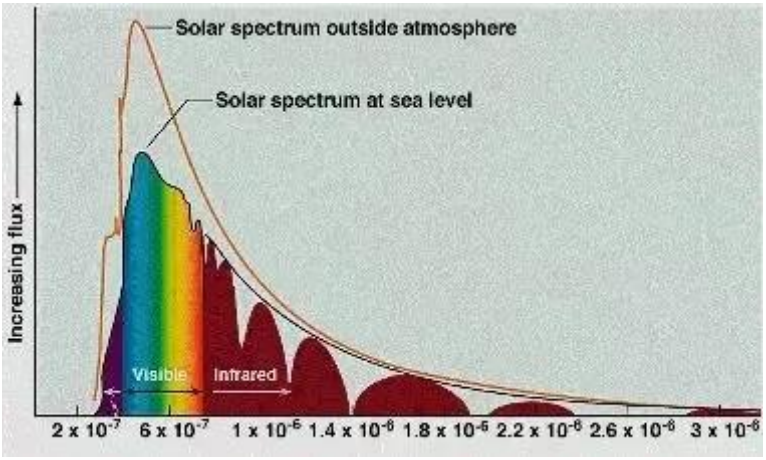

Figure I.2: Spectral distribution of solar radiation

I.2.3. Absorption

The wave theory (Maxwell's equation) or the corpuscular theory of light allows us to look at the exchanges between matter and light radiation. According to corpuscular theory, the quanta of energy associated with light radiation are called photons[1]. In quantum mechanics field, the energy of the photon corresponding to a given radiation is related to its wavelength by the relation:

$$Ep = h\nu = \frac{hc}{\lambda} = \frac{1{,}24}{\lambda} \qquad \text{(I. 2)}$$

λ: Wavelength of the radiation in µm.

v: Radiation frequency.

E_p: Energy of the photon.

h: Planck constant.

c: Speed of light.

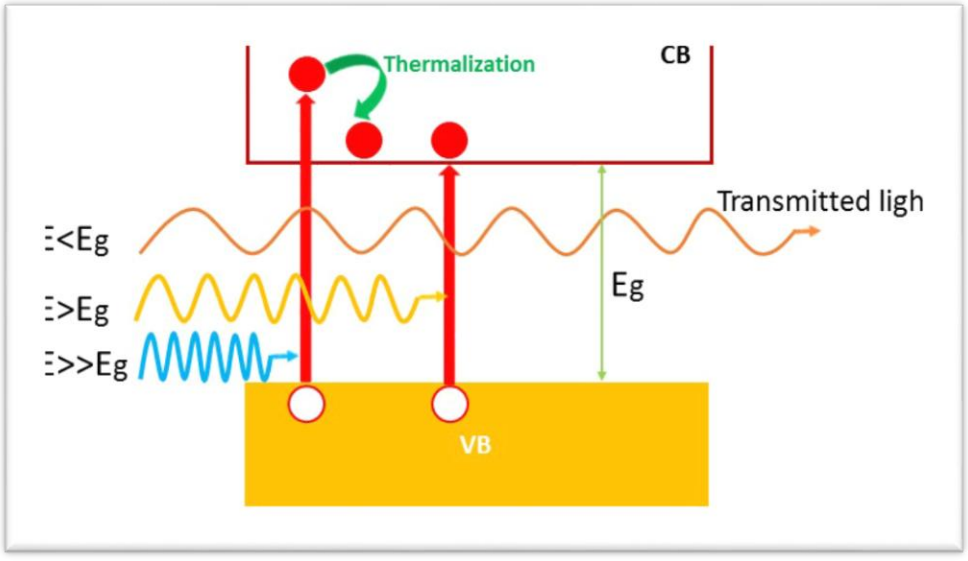

Figure I.3: Absorption system in a material.

Light absorption in a material follows a decreasing exponential law with respect to penetration depth:

$$I(\lambda) = I_0 e^{-\alpha x} \quad \textbf{(I. 3)}$$

With I_0 incident intensity, α [cm-1]: absorption coefficient and x [cm]: penetration depth. The absorption coefficient α depends on the wavelength of the incident photon. Absorption is a physical property of the material. In the case of solar cells for terrestrial applications, the ideal semiconductor material must strongly absorb the available wavelengths of the spectrum AM1. [3].

I.3. The photovoltaic cell

I.3.1. PV cell

The word "photovoltaic" (PV) is made up of two words: "photo-" meaning light and "-voltaic" (named after the Italian physicist Alessandro Volta (1745-1825) who discovered the first electrochemical battery) which means electricity. So, the definition of “photovoltaic conversion” is the direct transformation of light into electricity using a photovoltaic cell. The main inexhaustible source of light is the sun [5].

I.3.2. How the photovoltaic effect works

The photovoltaic effect used in solar cells directly allows to convert the light energy of the sun’s rays into electricity by producing and transporting, in the semiconductor, positive and negative electrical charges under the effect of light [2].

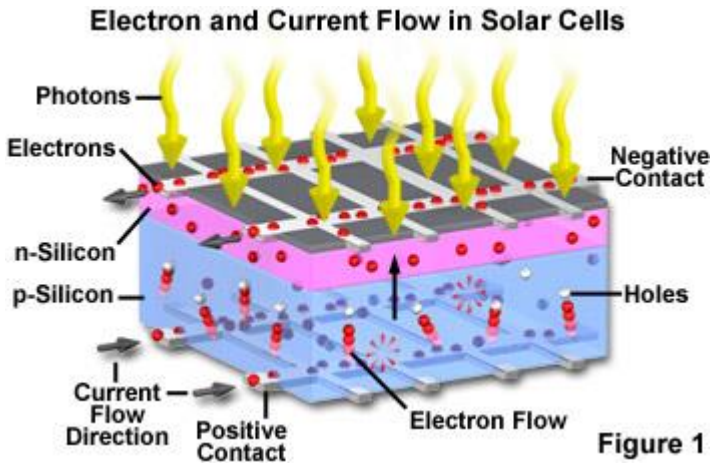

Figure I.4: Operating principle of the solar cell [6].

A PV cell is made from a semiconductor material. Its construction is comparable to that of a conventional diode. The cell is made of two different layers. The top layer is N-doped and the bottom layer is P-doped (Figure 1.4), creating a PN junction. This PN junction creates a potential barrier. When grains of light (photons) strike the surface of this material, they transfer their energy to the atoms of the material. This gain in energy releases electrons from the atoms, creating holes and electrons. This creates a potential difference between the two layers. This potential difference creates an E field that drains free the carriers towards the metallic contacts in the P and N regions. It results in an electric current and a potential difference in the PV cell. The current and voltage supplied by a PV cell depend on various parameters, which we will explain in the following [7].

I.4. Characteristics of a photovoltaic cell

I.4.1. Current-voltage characteristic (I-V)

Plotting the variation in current density as a function of voltage in a photovoltaic cell, under dim light and under illumination, provides access to a good number of physical parameters characteristic of the component.

Figure (1.5) demonstrate the current-voltage characteristic of a PN junction photovoltaic cell. In dim and in the ideal case, the curve obeys the following Shockley equation:

$$\mathbf{I = I_0[\exp(\frac{qV}{nKT}) - 1]} \qquad \mathbf{(I.4)}$$

Where $\mathbf{I_0}$ is the saturation current, q is the electron charge, K is Boltzmann's constant, T is the temperature, n is the diode ideality factor and V is the polarization potential (V) [8].

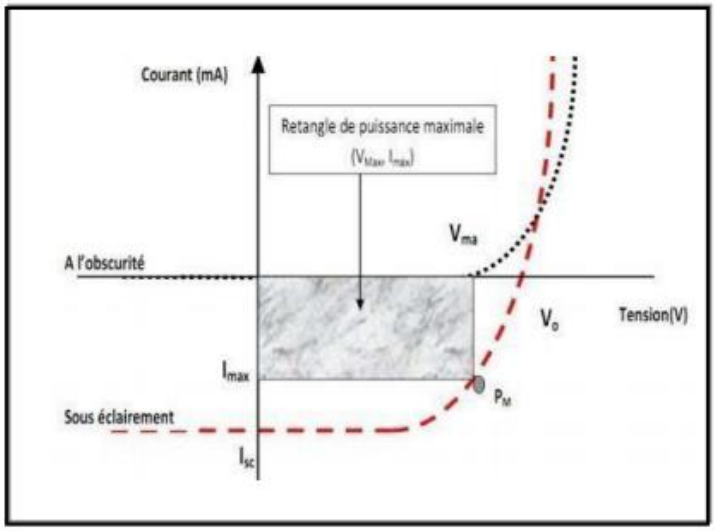

Figure I.5. Current-voltage characteristic of a photovoltaic cell under dim light and illumination.

I.4.2. Electrical parameters of a photovoltaic cell

The photovoltaic cell has a number of characteristics, the most important of which are:

- short-circuit current ***Jsc***.
- Open circuit voltage ***Voc***.
- The form factor ***FF.***
- Performance.
- The external quantum yields.

I.4.2.1 The short-circuit current density (J_{cc} or J_{sc})

This is the current density when the potential applied to the cell is null. It is the highest current density that the cell can supply. It is a function of temperature, the wavelength of the radiation, the active surface of the cell, the mobility of the carriers and is linearly dependent on the intensity of the received light.

I.4.2.2 The open circuit voltage (V_{co} or V_{oc})

This is the maximum potential that the cell can supply when the current is null. In the case of organic photovoltaic cells, the V_{oc} is a function of the **HOMO** level of the electron donor material and the **LUMO** level of the electron acceptor material. Charge losses at the material-electrode interfaces also affect this value.

I.4.2.3 The FF form factor

It is a ratio that reflects the quality of the shape of the current-voltage density characteristic. It is defined by the following relationship:

$$FF = \frac{P_{max}}{J_{sc} J_{oc}} = \frac{J_{max} \cdot V_{max}}{J_{sc} J_{oc}} \qquad \textbf{(I. 5)}$$

where J_{max} and V_{max} represent the current density-voltage pair for which the power delivered by the cell is maximum (P_{max}), and the theoretical FF formfactor is between 0.25 and 1.

The form factor FF can also give information about the quality of the material-electrode interfaces. When its value falls below 25%, this generally indicates the presence of a non-ohmic contact or an oxidized layer and/or insulation at the material-electrode interface.

I.4.2.4 The energy conversion efficiency

Defined by the ratio between the maximum energy delivered by the cell P_{max} and the incident light energy P_{in} :

$$\eta = \frac{P_{max}}{P_{in}} = \frac{FF \times V_{oc} \times I_{cc}}{P_{in}} \qquad \text{(I. 6)}$$

The maximum conversion efficiency of a cell doesn't have a meaningful context only for a given spectral distribution and intensity. The most commonly used standard illumination **(also used in this work)** corresponds to the AM1.5 standard [9].

I.4.2.5 Quantum Efficiency (quantum Yield)

The cell's Internal Quantum Efficiency (IQE) is defined as the number of electrons passing from the valence band to the conduction band per incident photon. It is written as:

$$\textbf{IQE} = \frac{J_{ph}}{q(1-R)E_{inc}} \qquad \text{(I. 7)}$$

Another interesting cell parameter, which is more accessible experimentally, is the **RS**. RS is the current generated by the cell in relation to the energy supplied per wavelength of incident radiation. It is expressed as follows:

$$\mathbf{RS} = \frac{q}{hc} \times IQE = \frac{q \times ne}{\frac{hc}{\lambda} \times n_{ph}} = \frac{I_{sc}}{P_{inc}} \qquad \textbf{(I. 8)}$$

Where **ne** is the electrons,flux short-circuited in the cell per time unit and n_{ph} is the photons' flux with a wavelength of **λ** arriving at the cell per time unit. **RS** is therefore the value of I_{sc} in the cell per unit of incident monochromatic flux. It can be accessed experimentally: use a calibrated diode (whose **RSd** curve is known) to measure the luminous flux, which will be noted as **φd** (flux on the diode). The current density generated by this diode is measured at each wavelength **Jd(λ)** we obtain the flux **φd(λ)** thanks to the following equation:

$$\mathbf{R}\, S_d(\lambda) = \frac{J(\lambda)}{\varphi_d(\lambda)} \qquad \textbf{(I. 9)}$$

We measure the current density generated by the sample at each wavelength **Jéch(λ)** and associate the flux received by the sample **φéch(φ)** which corresponds to that received by the diode, to within a coefficient **(k)**. This coefficient is due to the optical system not being perfectly symmetrical [10].

I.4.2.6 Equivalent electrical circuit of the photovoltaic cell

The simplest equivalent diagram of the photovoltaic cell with an ideal PN junction comprises a current source I_{Light} , which models the photoelectric current, associated with a diode in parallel which models the **P-N** junction, the polarization of which determines the voltage (Figure I.6).

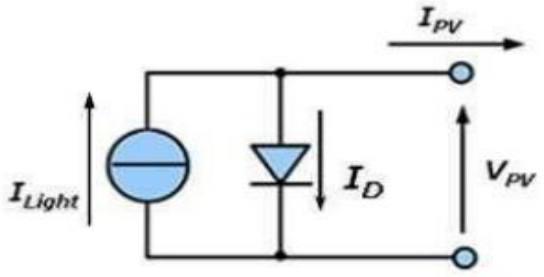

Figure I.6. Simplest equivalent diagram of the PN junction photovoltaic cell.

A more complete equivalent diagram of a photovoltaic solar cell (single diode model) is shown in the figure below. It completes the previous diagram by introducing two resistors, **R_{sh}** and **R_s**, which model the cell's defects.

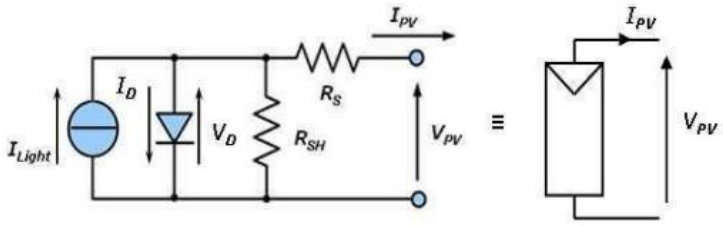

Figure 1.7: Equivalent circuit of a photovoltaic solar cell and conventional diagram of a photovoltaic cell or photovoltaic module.

- I_D = Diode reverse current.
- I_0 = Diode saturation current, temperature dependent.
- I_{Light} = Photocurrent, depending on the intensity of the irradiation.
- R_{SH} = Parallel resistance, representing the parallel admittance of the current generator.
- R_s = Resistance in series, modelling the ohmic losses of the material and contacts.
- V_{pv} = Cell voltage in its terminals.
- I_{pv} = Current supplied by the cell.

The operation of the circuit as a generator can thus be formalized by a system of equations resulting from Kirchhoff's laws.

$$I_{pv} = I_{Light} - I_0 \cdot \left[\exp\left(\frac{V_{pv}+(I_{pv}\cdot R_s)}{V_r}\right) - 1\right] \frac{V_{pv}+(I_{pv}\cdot R_s)}{R_{SH}} \qquad \textbf{(I. 10)}$$

With:

$$V_r = \frac{m.K.T}{q} \qquad \textbf{(I. 11)}$$

Where:

- m = Material index (between 1 and 2 depending on the technology).
- k = Boltzmann constant.
- T = Temperature in Kelvin.
- q = Charge of the electron.

A photovoltaic (PV) cell will therefore produce energy in proportion to the light intensity it receives. Temperature is also a factor influencing the I-V characteristics of a photovoltaic cell[11].

I.5. Photovoltaic technologies

Solar cells are divided into three generations, the most important of which are:

I.5.1. First generation: solar cells based on silicon

There are two families that can be distinguished in the silicon industry are monocrystalline and polycrystalline silicon.

a) Monocrystalline silicon

Monocrystalline silicon consists of a single crystal, with a uniform bluish-grey and sometimes black appearance. It is made from a very pure block of silicon, formed from a single crystal. The industrial process for obtaining it is cumbersome and costly, but it can produce cells with an efficiency of around 20% [12].

In the lab, the best efficiency for this technology is 26.3%, while the efficiency of commercial modules is around 17 to 18% [1]. **Figure 1.8** shows a monocrystalline silicon cell.

Figure I.8. Monocrystalline silicon cell [13].

b) Polycrystalline silicon

Polycrystalline silicon is produced by several techniques that ensure the formation of a columnar structure with large crystals (known as multi-crystalline silicon) in order to limit the harmful effects of grain boundaries. However, the multi-crystalline material is both stressed and dislocated, and contaminated by residual impurities in the silicon raw material. Some of this raw material is scrap from the microelectronics industry, i.e., monocrystalline **Cz** or **FZ** silicon. Industrial conversion yields, which were of the order of 8 to 10% before 1980, are currently 16 to 17% for large panels of 200cm² [14].

Crystalline poly with a yield of **η** ~14 to 18% (in 2015). It is prepared by heating amorphous **Si** followed by cooling (crystalline by domain). Its advantage is its high efficiency (at 100W/cm² in full sunlight), which is cheaper than monocrystalline, but its limited efficiency in low light conditions. It is found in the solar panels now used by almost all private individuals where **η** ~ 16 to 24% (2015) [1].

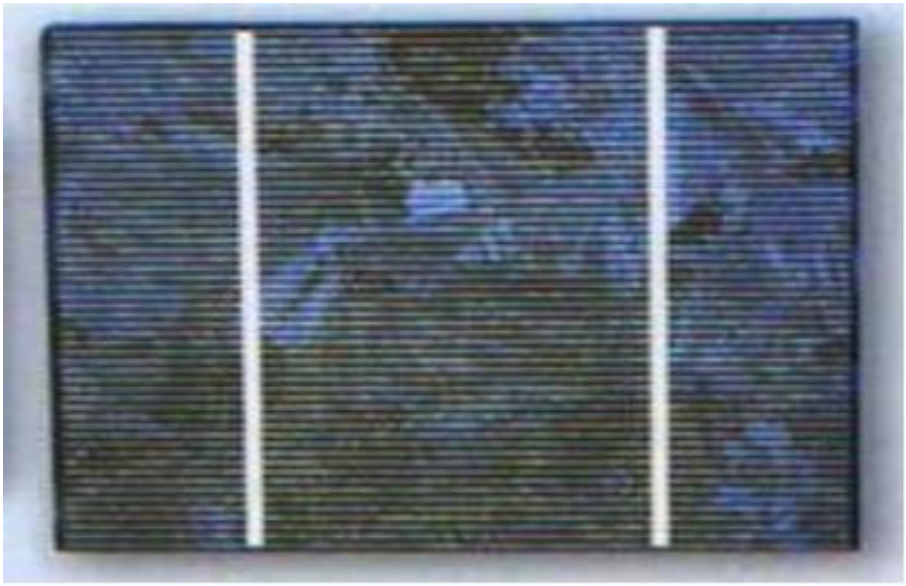

Figure I.9: Polycrystalline cell [18].

Table I-1: 1st generation solar cells [5].

Solar Cell	Surface area (cm²)	Yield (%)
Mono-crystalline silicon	180.43	26.3 ± 0.5
Multi-crystalline silicon	242.74	21.3 ± 0.4

I.5.2. Second generation solar cells

a) Amorphous silicon

Amorphous silicon shown in Figure I.10 first appeared in 1976. Its atomic structure is disordered and uncrystallized, but it has a higher absorption coefficient than crystalline silicon. However, what it gains in absorption power, it loses in electric charge mobility (low conversion efficiency).

- Much lower production costs.
- Efficiency of just 5% per module and 14% in the laboratory.
- Works in very low light [15].

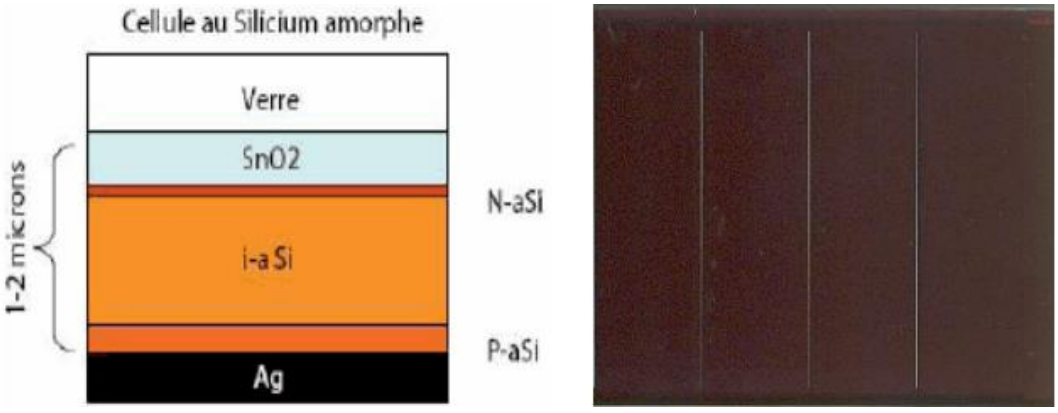

Figure I.10: Amorphous silicon cell[15 16] .

The chalcopyrite's **Cu(In,Ga)Se** (**CGIS**) are very promising materials for thin-film solar cells. They comprise several parts: an absorbent layer of **CGIS**, a metal used as the cathode and a transparent material as the anode. The best performance achieved with these cells deposited on glass is 20.3%, while Swiss researchers at the Swiss Federal Materials Testing Laboratory have developed flexible solar cells on flexible plastic sheets, with a new record conversion rate of 20.4%, higher than the 18.7% obtained by the same team in May 2011.

Despite these advances, the price of these cells is high because of the scarcity of indium and gallium, so a reduction in the thickness of the absorber layer (between 1.5- 2µm) is necessary. To achieve this, absorber layers less than 0.5µm thick have been fabricated, and the results show a slight reduction in the open circuit voltage **Voc** and the form factor, but the short circuit current density has decreased significantly [17]. **Figure I.11** shows a **CIGS** solar cell.

Figure I.11: CIGS solar cell [18].

c) Cadmium telluride (CdTe)

It is a promising material for thin-film solar cells because of a direct bandgap of around **1.5eV** and a high absorption coefficient (**>5x105 /cm**). The energy conversion record for thin-film cells based on polycrystalline **CdTe** is equal to 17.3%. However, this record is well below its theoretical maximum efficiency (~29%), possibly due to problems with the P-N junction interface between **CdS** and **CdTe**. It has also been shown that the formation of a **CdS1-xTex**

solid solution, with a low bandgap, affects the photovoltaic parameters of **CdS/CdTe** cells [12], and that interfaces and charge recombination decrease the Performance.

Table I-2: Examples of second-generation solar cells [8].

Solar cell	Surface area (cm^2)	Yield (%)
CIGS	0.9927	21.0 ± 0.6
CdTe	1.0623	21.0 ± 0.4
Amorphous silicon	1.001	10.2 ± 0.3

The figure below shows a cadmium solar cell:

Figure I.12: Cadmium solar cell [19].

I.5.3. Third-generation solar cells

a) Organic cells

Organic cells: This type of cell consists of an active layer, which in turn consists of several polymer layers (**Figure I.16**). This active layer is sandwiched between two conductive layers. Generally, one of these layers is transparent and not more than 10nm thick. They are still in the research stage with yields not exceeding 5 [20]. **Figure I.13** shows an organic solar cell.

Figure I.13. Organic solar cells [20].

b) Perovskite cell

This element is most often embodied by an organic-inorganic lead hybrid or a tin halide (in its active layer). Going from 3.8% in 2009 to 22.1% in 2016.The advent of hybrid perovskite has amazed research groups in the photovoltaic sector, as it has demonstrated high performance and rapid growth over the last 5 years. These materials have led to an increase in power conversion efficiency (PCE) for photovoltaic (PV) devices of over 20% . [20]**Figure I.14** shows a Perovskite solar cell.

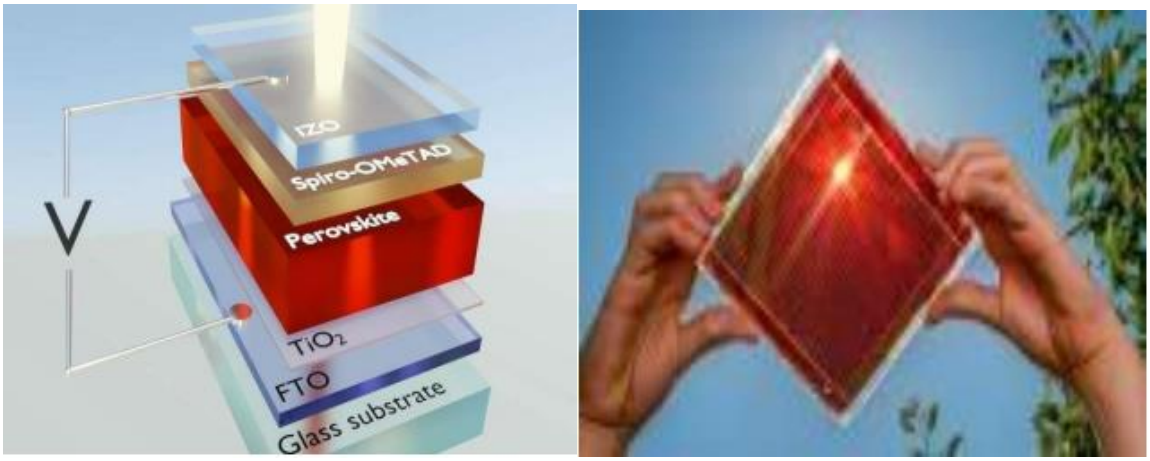

Figure I.14: Perovskite solar cell [21] [22].

Table I-3: Examples of 3rd generation solar cells [5].

Solar cell	Surface area (cm2)	Yield (%)
Organic	0.992	11.2 ± 0.3o
Perovskite/Si(monolithic)	0.990	± 0.6

I.6. Advantages of using photovoltaic cells

Here are the advantages that make photovoltaic cells an efficient source of renewable energy:

- The conversion of electricity from sunlight or solar radiation is direct. So there's no need to install a bulky generator.
- Solar power generation is environmentally friendly. A photovoltaic panel supplies clean, green energy. There are no gas emissions when electricity is produced.
- Free from the use of fuel and water.
- Solar energy is generated by nature, and is free and simple.
- Wherever sunlight is available, solar energy can be easily generated.
- Photovoltaic energy is well suited to smart energy networks with distributed electricity production.
- Photovoltaic cells have no mechanically moving parts like wind turbines, so they are less likely to break and require less maintenance than other renewable energy sources.
- Photovoltaic panels are totally silent and produce no noise.
- They can be used in remote areas where the installation of an electric grid is too costly.
- Photovoltaic panels can easily be installed on the ground or on roofs of residents' homes without the interference in their livelihood.
- They have a long lifespan, up to 30 years [18].

I.7. Conclusion

In this chapter, we have presented a general study of the solar cell and the photovoltaic cell. Thanks to our study, we have discovered that solar cells convert the energy of solar radiation directly into electricity. One of the materials used in the solar cell is perovskite, which we will discuss in the second chapter.

CHAPTER II ADVANCEMENTS IN PHOTOVOLTAIC SOLAR CELLS

CHAPTER II ADVENCEMENT IN PHOTOVOLTAIC SOLAR CELL

II.1. Introduction

This chapter delves into the exciting field of photovoltaics, focusing on the utilization of SCAPS 1-D software and the development of advanced solar cell technologies. SCAPS 1-D software has emerged as a powerful tool for simulating and optimizing solar cell performance, allowing researchers to explore various parameters and device configurations in a virtual environment. One area of particular interest is the application of perovskite materials, such as CsPbI2Br, which have demonstrated remarkable optoelectronic properties and hold great promise for next-generation solar cells. Additionally, the selection and optimization of hole transport layers (HTL) and electron transport layers (ETL) are critical in achieving efficient charge transport within the solar cell device. Furthermore, the integration of CZTS (Cu2ZnSnS4) with silicon in a heterojunction architecture has garnered attention for its potential to deliver cost-effective solar cells with enhanced performance. This chapter explores the significance of SCAPS 1-D software, the role of perovskite materials, the importance of HTL and ETL, and the prospects of CZTS/silicon heterojunctions in advancing solar cell technology.

II.2. Introduction to SCAPS

Over the years, the advancement of numerical models has made numerical simulation techniques for solar cell devices increasingly reliable. These techniques have become essential for studying and comprehending the properties of solar cells. Through these models, a better understanding of the underlying mechanisms of solar cells has been achieved, facilitating the development of cells with improved efficiency and performance. we begins by introducing the mathematical equations employed to describe the functioning of solar cells[23]. Subsequently, the solar cell simulation software (SCAPS) utilized in our research will be described.

II.2.1. Basic equations

In order to accurately model the electrical properties of solar cells, the SCAPS software numerically solves the basic equations of semiconductors using the drift-diffusion approximation.

II.2.2. Poisson equation

The Poisson's equation is used to describe the relationship between potential and spatial charges.

$$\frac{\delta\phi}{\delta x} = qe[n(x) - p(x) - N^{+}(x) + N^{-} - p(x) + n(x)] \quad \text{(II.1)}$$

Where φ is the potential, q is the elementary charge, ε is the permittivity, n is the density of free electrons, p is the density of free holes, ND is the donor doping density, NA is the acceptor doping density, pt is the density of trapped holes, and nt is the density of trapped electrons.

II.2.3. Continuity equations

These equations allow for the simultaneous analysis of carrier drift, diffusion, generation, and recombination.

$$\frac{\delta n}{\delta} = \frac{1}{q}\nabla.Jn + G_n - R_p \quad \text{(II.2)}$$

$$\frac{\delta p}{\delta} = \frac{1}{q}\nabla.Jp + G_P - R_P \quad \text{(II.3)}$$

Where Gn (Gp) is the optical generation rate of electrons (holes), and Rn (Rp) is the recombination rate of electrons (holes).

Jn, Jp are the electron and hole current densities given by the transport equations (II.4) and (II.5)

$$J_n = -qn\mu_n\nabla\Psi + qD_n\nabla n \quad \text{(II.4)}$$

$$J_p = -qp\mu_p\nabla\Psi + qD_p\nabla p \quad \text{(II.5)}$$

Where q is the elementary charge, μn (p) is the electron (hole) mobility, and Dn (p) is the electron (hole) diffusion coefficient.

The diffusion coefficient depends on the carrier mobility as shown in equations (II.6) and (II.7).

$$Dn = \frac{\mu_n k_b T}{q} \quad \text{(II.6)}$$

$$Dp = \frac{\mu_P k_b T}{q} \quad \text{(II.7)}$$

Where K_b is the Boltzmann constant and T is the temperature.

II.2.4. Diffusion length

The diffusion length describes the carrier transport capability in a solar cell device. It depends on the diffusion coefficient and the carrier lifetime. This is represented in equations (II.8) and (II.9).

$$l_n = \sqrt{D_n\tau_n} \quad \text{(II.8)}$$

$$l_p = \sqrt{D_p\tau_p} \quad \text{(II.9)}$$

Where $L(n)$ ($L(p)$) is the electron (hole) diffusion length, and rn (rp) is the electron (hole) lifetime [23].

II.3. SCAPS software

The simulation of thin-film solar cells has become increasingly popular in recent years, leading to the development of several calculation and simulation software tools by the research community in this field. Examples of such software include AMPS-1D, PC-1D, ASA, SCAPS-1D, SILVACO, and more. SCAPS-1D, which stands for "Solar Cell Capacitance Simulator One Dimension," is a program developed at Ghent University in Belgium using Windows/CVI National Instruments by Marc Burgelman et al. This program ise specifically designed for

simulating photonic devices such as CdTe and CIGS solar cells [24].Some of the key advantages of SCAPS-1D includ:

- The input files are accessible to the user in text format, including spectral data and parameters describing the device.
- Possibility to introduce interfaces and take into account the recombination phenomenon within them.
- Introduction of series resistances and obtaining capacitance-voltage and capacitance-frequency characteristics.
- It is a software that offers high execution speed

II.3.1. Interface of the SCAPS software

The interface of the SCAPS-1D software's startup panel, called the action panel, is the main window of SCAPS (Figure III.1). In this panel, all the external simulation parameters can be controlled, such as temperature, voltage, frequency, solar light, etc. The action panel can be divided into six sections or parts, which can be described as follows [23]:

- Section (1) "Define the Problem" is dedicated to defining the problem of the structure, materials, and all physical properties of the simulated solar cell.
- Section (2) represented as "Action" where external electrical conditions can be controlled, such as the starting point of applied bias, step size, final voltage, frequency, etc.
- Section (3) represented as "Illumination" is dedicated to selecting light and dark conditions and the type of spectrum for the simulation.
- Section (4) is the "Operating Point" where the operating point values such as temperature can be specified, along with the specification of series or shunt resistances if needed.
- Section (5), represented by "Calculate," allows initiating the calculation process of the simulated device.

- Section (6), represented by "Calculation Results," serves the purpose of displaying curves and results of the simulated device.

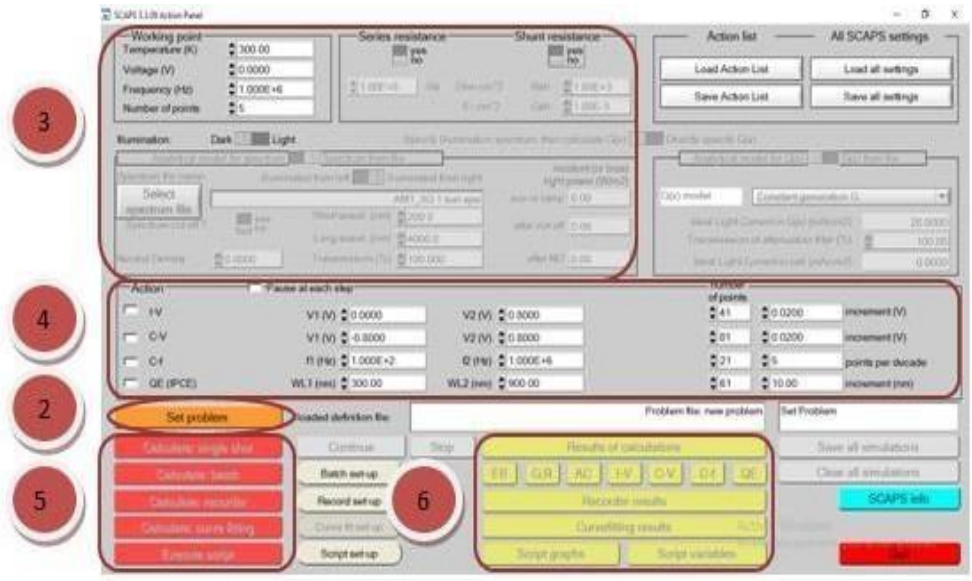

Figure II.1. "Action Panel" is the execution window of the SCAPS software

II.3.2. Set operating point

The operating point specifies the important simulation parameters.

- Temperature T: Important for all measurements.

  Note: in SCAPS, Nc(T), Nv(T), thermal velocities, thermal voltage KT, and all their derivatives are the only variables that have an explicit thermal dependence; for each T value, the corresponding material parameters must be manually entered.

- Voltage V: It does not apply to I-V and C-V simulations. It is the DC bias voltage in a C-f and QE(λ) simulation. SCAPS always starts at 0 V and runs up to the operating point voltage in a specified number of steps. Frequency f: It does not apply to I-V, QE(λ), and C-f simulations. It is the frequency at which the C-V characteristic is simulated.

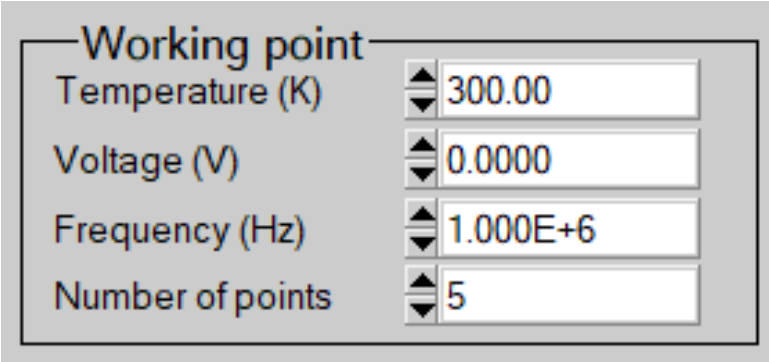

Figure II.2. Definition of the operating point**.**

- Illumination plays a crucial role in all measurements. In the case of QE(λ), it determines the polarization conditions of the light. The key parameters include darkness or light, the selection of the illuminated side, and the choice of the spectrum. The default spectrum used is the solar spectrum with a global air mass of 1.5 and an intensity of 1000 W/m2. However, there is also a wide range of options available, including monochromatic lights and custom spectra for more specific simulations. Additionally, if an optical simulator is accessible, it is possible to load a generation profile instead of relying on a predefined spectrum.
- Nombre des points : Le nombre des points utilisé pour tracer les courbes.

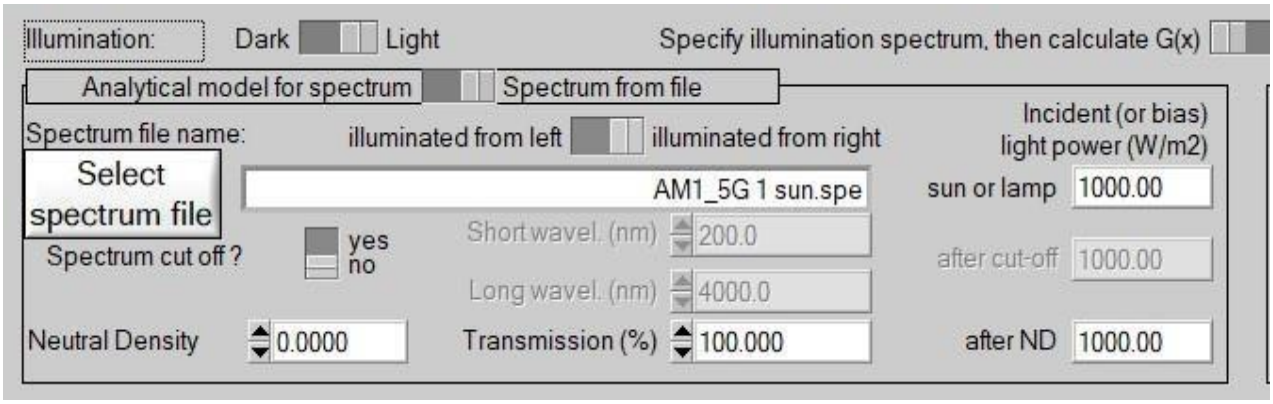

Figure II.3. illumination choice.

II.3.3. Device design window (Set Problem)

To define the problem, including the geometry, materials, and all properties of the solar cell, you need to click on the "Set Problem" button on the action panel. This action opens a new

window, which is the solar cell definition panel (Figure II.4). This interface plays a crucial role in the simulation of the cell. In this panel, you can create different layers and define their physical parameters and properties. You can also visualize the device structure.

The device definition interface has three parts, each with specific details:

- Section (1): In this part, we can define structures consisting of up to 9 layers. The first layer is the back contact, and the last layer is the front contact. The user can specify the properties of all layers.
- Section (2): This displays the defined structure of the photovoltaic device with front and back contacts. There are additional buttons for selecting the device illumination from either the back contact side or the front contact side, the direction of applied voltage to the device, and a dedicated button to reverse the layer order of the structure.
- Section (3): This section includes buttons to save the definition file in the SCAPS library or an external library, as well as load previously saved structure definition files. The buttons for Cancel and OK are also present.

These buttons allow you to exit or enter the device definition interface and return to the startup interface.

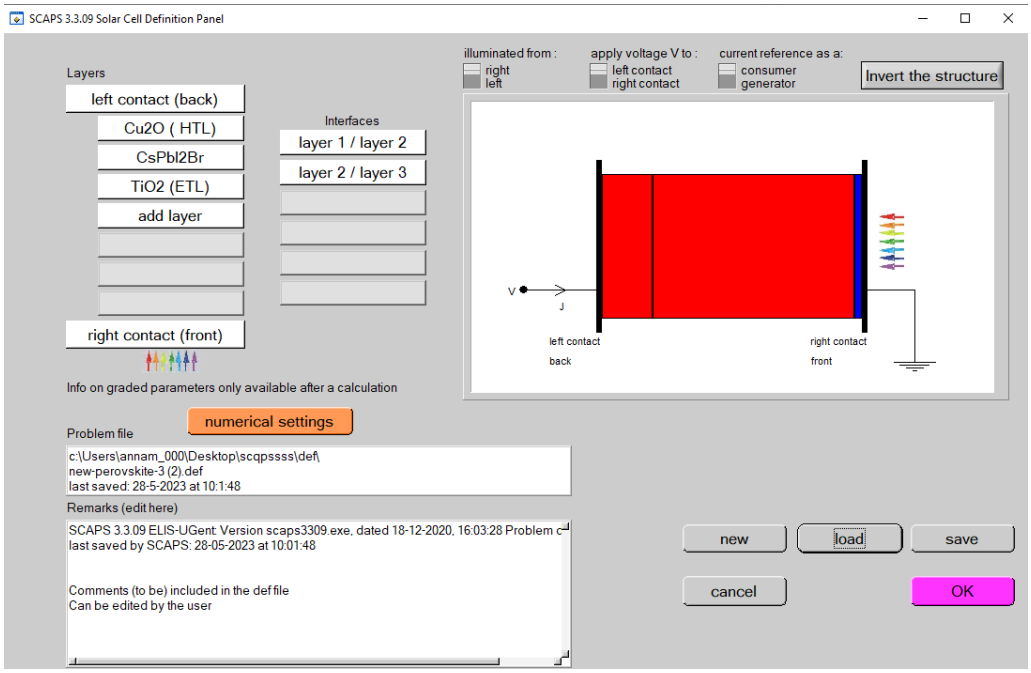

Figure II.4. Solar Cell Layer Definition Interface.

II.3.4. Editing the structure of a solar cell

When you click on the "SET PROBLEM" button on the action panel, the "SOLAR CELL DEFINITION" panel will appear. This panel allows you to create or modify the structures of solar cells and save or load them from other files. These definition files are standard ASCII (American Standard Code for Information Interchange) files with a ".def" extension that can be opened with Notepad.exe or Wordpad.exe. It is not recommended to modify these files, as it may render them unusable.

The properties of layers, contacts, and interfaces can be modified by clicking on the appropriate button, as shown in Figure II.4. Similarly, layers can be added by clicking on "ADD LAYER".

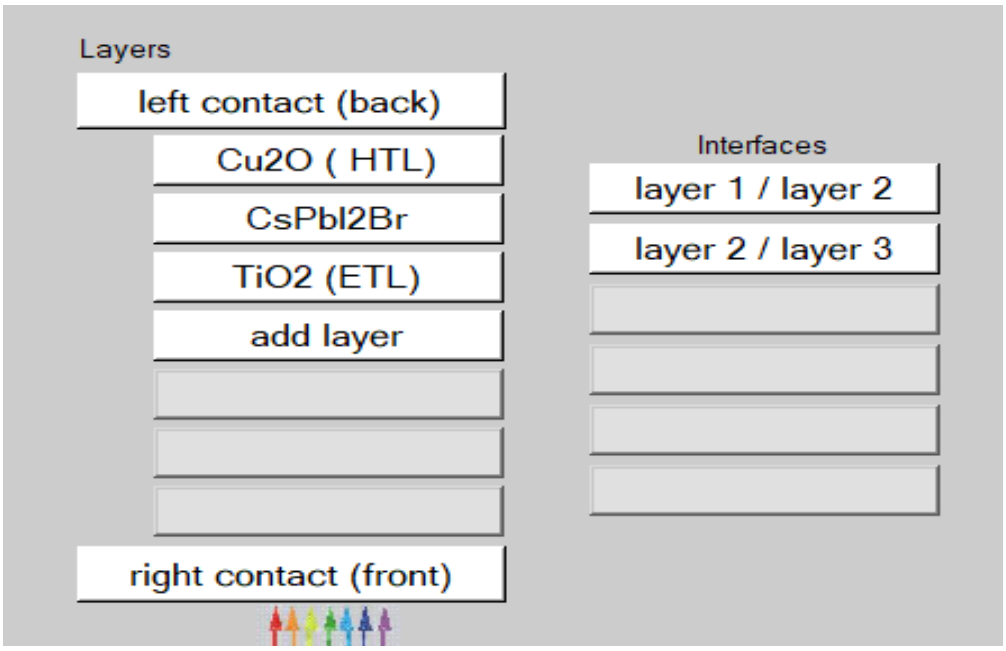

Figure II.5. Definition of solar cell structure.

II.3.5. Defects

Defects can be defined by clicking on the "add defect" button in the layer properties definition panel. This panel also allows for defining recombination models.

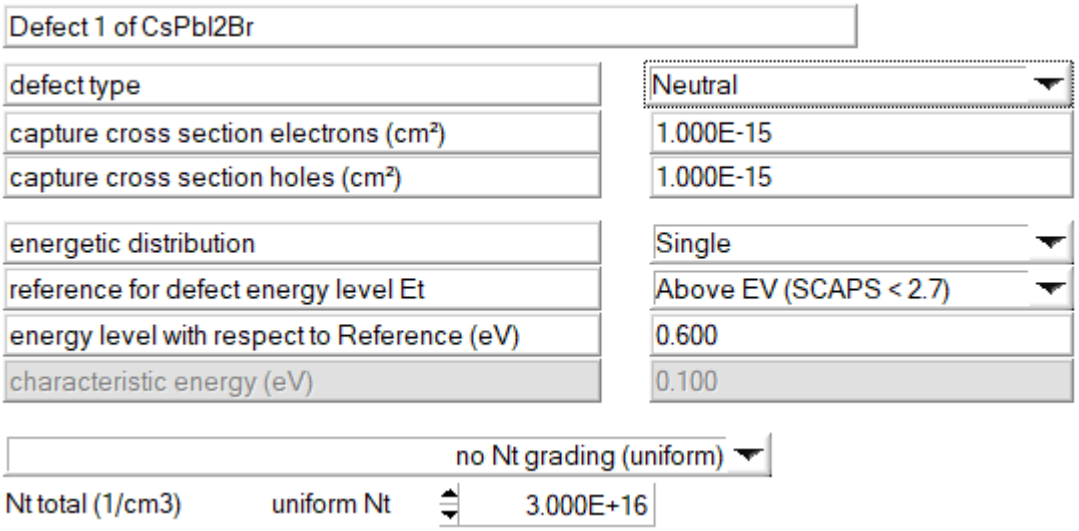

Figure II.6. Default properties definition panels.

II.3.6. Solar cell layer definition

By clicking on the "add layer" button in the Solar Cell Definition Panel view, a window opens that contains various parameters of the material to be entered, as shown in FigureIII.9. These parameters can have uniform or non-uniform distributions based on the physics of the material. The properties of the layer are as follows, from top to bottom

The properties of the layer, from top to bottom, include

- Layer name (corresponding to the doping type): This is where you can specify the name of the layer, which corresponds to the type of doping.
- Layer thickness: You can define the thickness of the layer.
- Material purity and profile: This refers to the purity of the material used in the layer and its profile.
- Energy gap, electron affinity, relative dielectric permittivity, effective densities of the conduction and valence bands, thermal velocities of electrons and free holes, electron and hole mobilities: These parameters describe the electrical and transport properties of the layer. They include the energy gap (bandgap), electron affinity, relative dielectric permittivity, effective densities of the conduction and valence bands, thermal velocities of electrons and free holes, and the mobilities of electrons and holes.
- Effective masses of electrons and holes (considering carrier transport by tunneling): If carrier transport by tunneling is taken into account, the effective masses of electrons and holes can be specified.

- If the material is a compound of elements with non-uniform concentrations, you can introduce gradual variations in the previous parameters.

- Doping type and density: The type of doping and its density can be introduced as uniform or with gradual variations, such as linear or parabolic profiles.

Layer absorption: The absorption of the layer, as shown in Figure III.10, can be defined using the analytical model provided by SCAPS, or it can be introduced as data. SCAPS provides absorption data for various semiconductor types.

- Alternatively, you can use absorption data for semiconductors not available in SCAPS, as long as the file has the same extension as the absorption files provided by SCAPS.

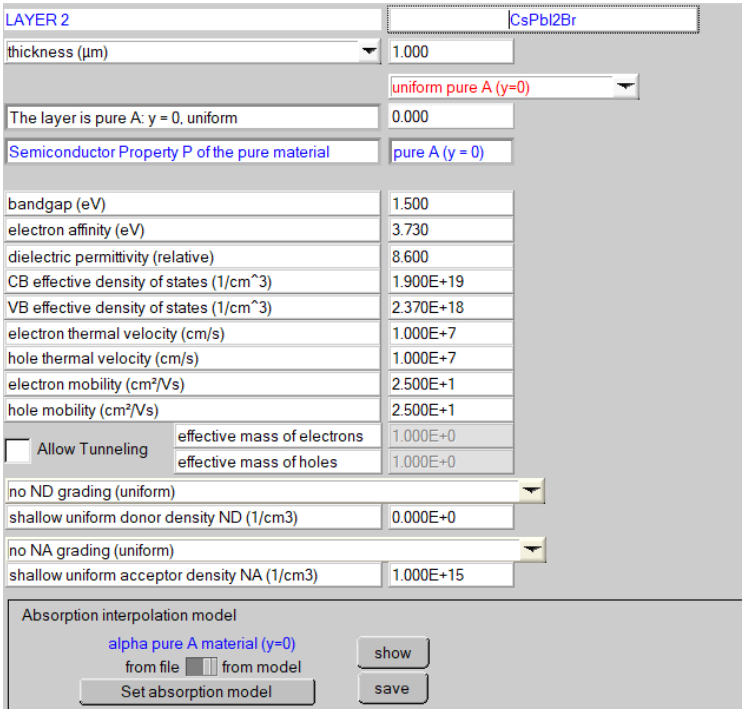

Figure II.7. Properties of the added layer

The types of bulk recombination present are indicated on the right side of the layer properties panel, as shown in Figure III.11. All types of recombination, whether direct or through traps, are accounted for.

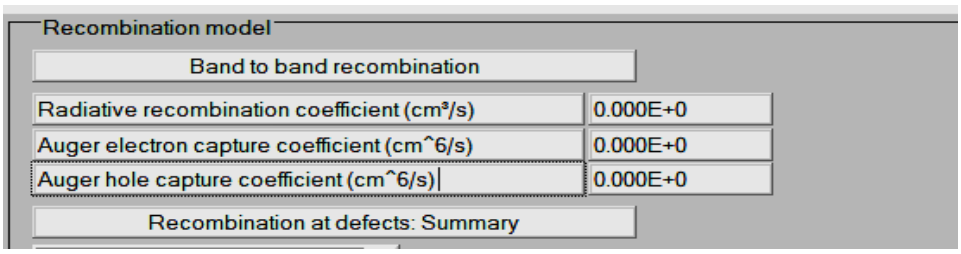

Figure II.8. Types of recombination, either direct or through traps**.**

II.3.7. Result window

After inputting all the necessary data (solar cell configuration, layer properties, and material properties), the "Calculate" button in the action panel interface can be clicked to start the simulation. As a result, the energy band panel opens, and the calculations begin. This window displays the simulation results in the form of graphs, with the option to save or export the values. SCAPS is capable of calculating energy bands, concentrations, currents at a given operating point, I-V characteristics, C-V characteristics, C-f characteristics, quantum efficiency (QE), and energy bands under alternating conditions.

II.3.8. Selection of measurements to simulate

In the "Action" section of the action panel, you can choose one or more measurements to simulate: IV (current-voltage), C-V (capacitance-voltage), C-f (capacitance-frequency), and QE(λ) (quantum efficiency as a function of wavelength). You can also adjust the initial and final values of the parameter, as well as the number of steps.

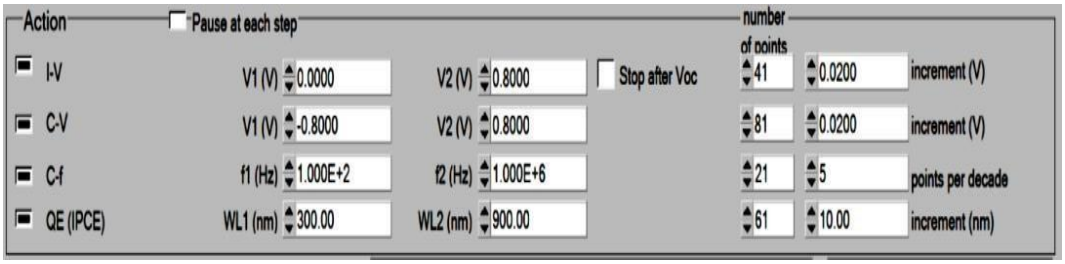

Figure II.9. section of the action panel

II.3.9. Display the simulated curves

After the calculations, SCAPS switches to the energy band panel as shown in Figure II.10. In this panel, you can view band diagrams, free carrier densities, and current density at the final polarization point. If you want to display the results for intermediate voltages, you can use the "Pause" button in the action panel. The results can be displayed using commands such as PRINT, SAVE GRAPHS, and SHOW, and the values will be shown on the screen. You can also copy and paste the results to other programs like Excel or save the values in a data file. If you have simulated at least one measurement operation, you can switch to custom panels as well [24]

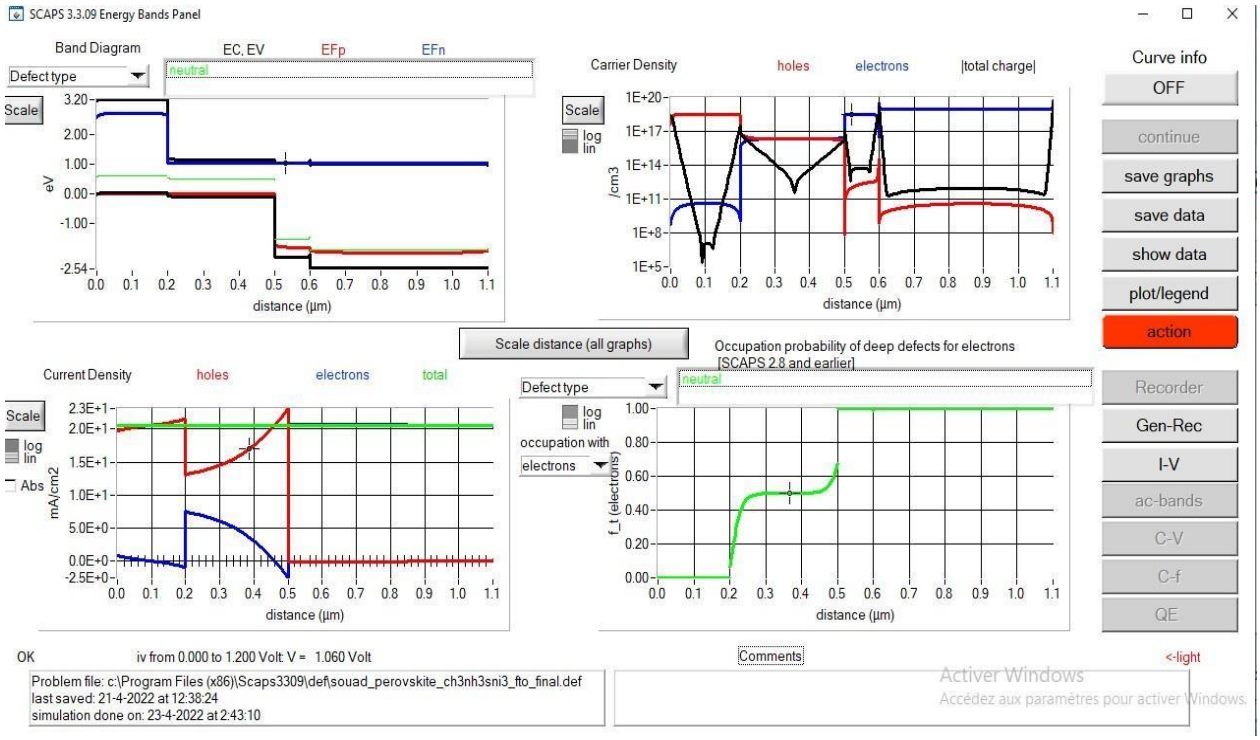

Figure II.10. Energy band panel**.**

II.3.10. I-V curves

Figure II.11 shows the display panel for I-V curves in the dark and under illumination. The color of the last calculated curve is indicated (when the graph becomes too crowded, you can click "Clear All Graphs" in the action panel). Recombination rate curves are only displayed for the last simulation. The legend color corresponds to the color of the curve. If "Curve Info" is set to ON and you click on a curve in the graph, a pop-up panel will appear with information about the graph, curve, and the clicked point.

The "Scale" button helps to change the range and scale of the axes. If you press the CTRL button and select a rectangular area in a graph, it will zoom in (enlarge) into the selected area. Pressing the CTRL button along with a right-click will provide an outer zoom (Zoom out).

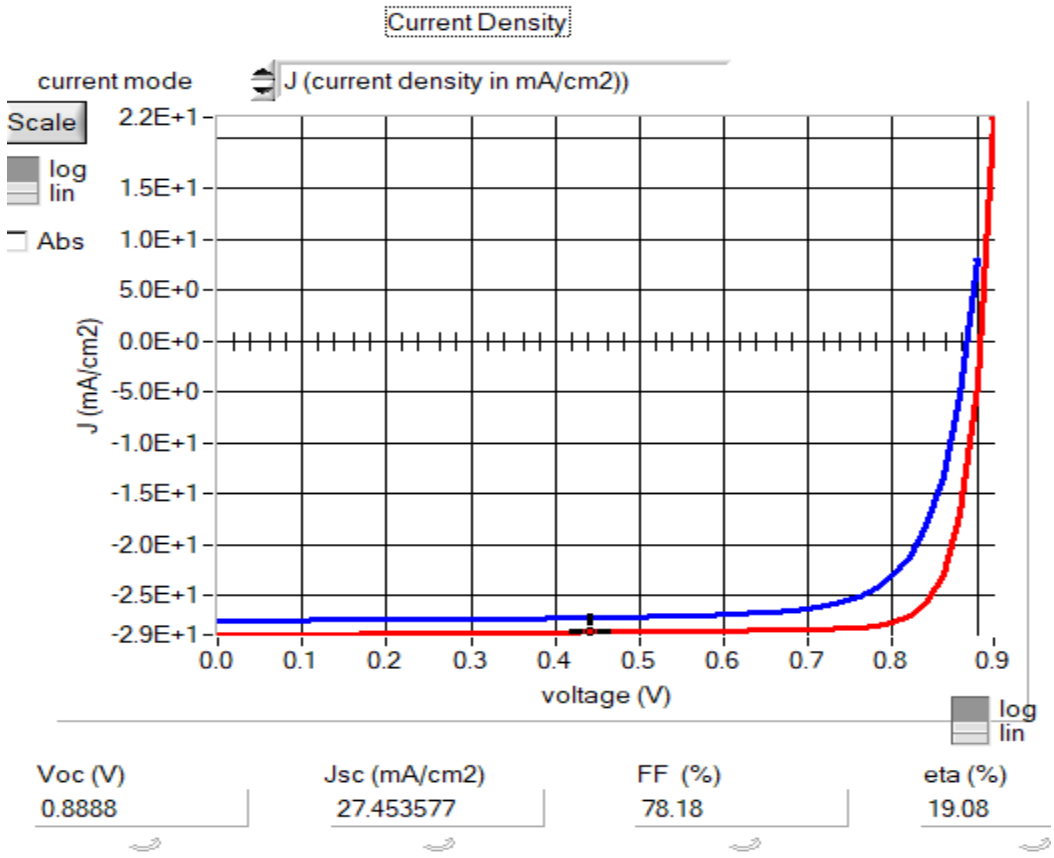

Figure II.11 Panel for displaying I-V curves under illumination.

II.4. Introduction to perovskite

Perovskite solar cells represent a type of solar device that employs perovskite-based materials as the light-absorbing layer. The utilization of inorganic-organic hybrid perovskite materials in liquid dye solar cells first emerged in 2009. This breakthrough was followed by a surge in research articles as the power conversion efficiency reached a notable 15% in 2013.Subsequent advancements led to even higher efficiencies, with the certified record standing at 22.1% and reported efficiencies peaking at 27.3% by 2017. Perovskite solar cells have outpaced desensitized and organic solar cells, aiming to match the efficiency of monocrystalline silicon cells. The low cost and ease of manufacturing perovskite solar cells offer significant advantages for both scientific research and industrial applications[25].

II.4.1. History and development

The first traces of halide perovskites date back to the last century, with initial articles on CsPbX3 family crystallizing in a perovskite structure and exhibiting photoconductivity properties as early as 1958. Subsequently, in the 1980s, the MAPbX3 family was synthesized, and studies on ionic conductivity in $CsPbX_3$ were reported. However, it was only in 2009 that this material was employed as an active material in a solar cell structure, achieving an efficiency of less than 4% but facing stability issues. As a result, it did not generate significant interest within the solar cell research community[26]. It was around 2012 when various research efforts coincided, demonstrating perovskite-based solar cells with efficiencies around 10%, that interest in perovskites surged (see Figure II.12). Since then, halide perovskites have attracted a tremendous global research community, these materials have emerged as one of the most promising contenders for the development of next-generation solar cells, with efficiencies reaching close to 25% in 2021 for perovskite-based polycrystalline thin-film solar cells. The history of colloidal perovskite nanocrystals (PNCs), on the other hand, stems from the success of nanocrystalline forms of conventional semiconductors such as CdSe, CdTe, PbSe, and their counterparts.

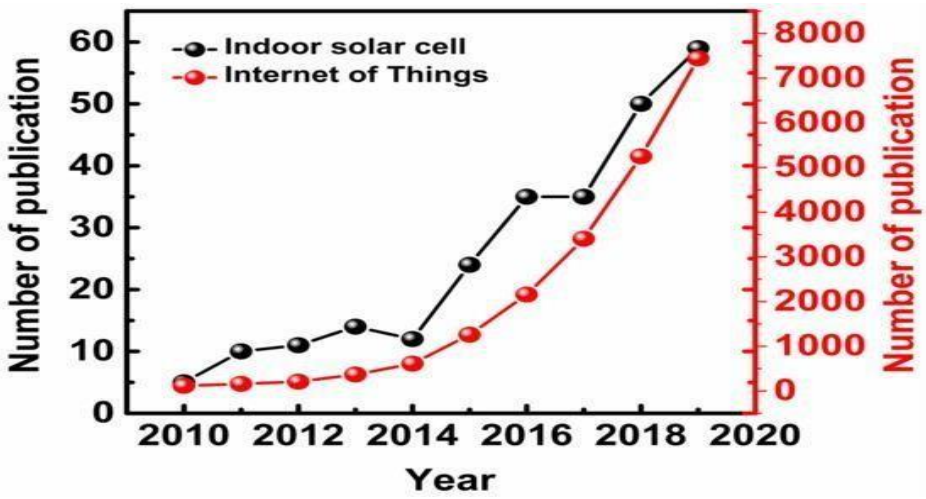

Figure II.12. Number of publications with the keyword “perovskite solar cell" over time

The advantageous properties of PNCs include their ease of synthesis and deposition, improved stability of the crystalline phase at room temperature, and high photoluminescence efficiency across the visible spectrum, all without the need for complex core-shell structures

typically associated with conventional colloidal semiconductor nanocrystals. This enhanced stability of the crystalline phase in PNCs, compared to polycrystalline films, also facilitates their rapid integration into solar devices. Remarkably, just one year after their synthesis, PNC-based solar cells achieved conversion efficiencies of slightly over 10%, and they have now reached efficiencies of 16.6%, approaching those of polycrystalline thin-film-based cells. This rapid increase in efficiency in PNC-based cells is accompanied by a significant improvement in the stability of cell performance (Fig. II.13).

Indeed, a $FAPbI_3$ nanocrystal cell maintains 100% of its efficiency for over a month, whereas a polycrystalline thin-film cell based on FAPbI3 will have lost 70% of its efficiency. These various advantages of nanocrystals make them an extremely promising material for optoelectronic applications, particularly in the field of solar cells [27].

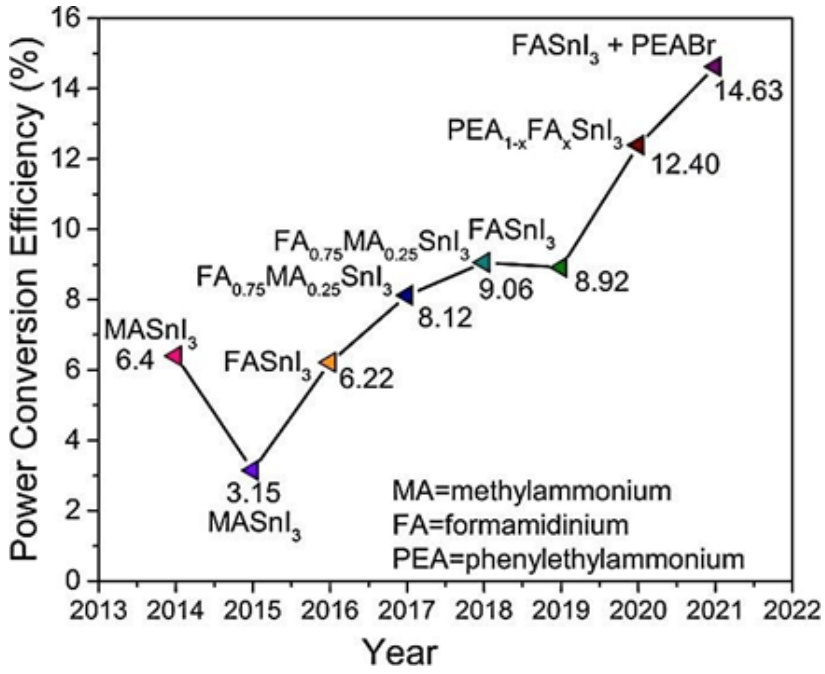

FigureII.13. Annual improvement in the efficiency of perovskite solar cell

II.4.2. Crystal structure of perovskites

The mineral perovskite, known as calcium titanate ($CaTiO_3$), was first discovered in 1839 by German mineralogist Gustav Rose. It is named after the Russian mineralogist Lev Perovskite. This crystal structure, represented in Figure II.14, is characterized by its chemical

formula ABX_3 and can accommodate various combinations of elements. Perovskite minerals are the most abundant class of minerals on Earth. In this structure, the A cation occupies the eight corners of a cube surrounded by twelve X anions, while the B cation is situated at the center of an octahedron formed by six X anions [BX6], located at the centers of the cube's faces[26] .

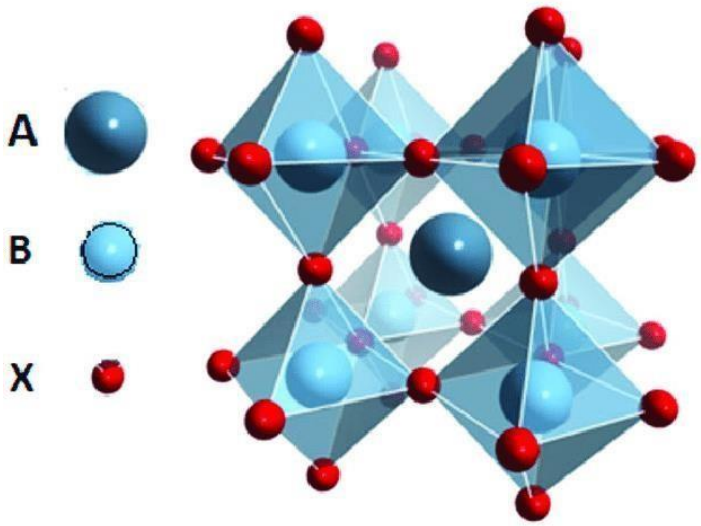

Figure II.14. Cubic structure of perovskite

There are two main categories of perovskites: inorganic perovskites, which consist of oxides, and halide perovskites, which can be either inorganic or hybrid (organic-inorganic). Table II.1 provides an overview of the different compounds associated with each type of perovskite [28].

Table II.1. The different molecules corresponding to the various families of perovskite [28].

	Oxyde	Halogénées inorganique	Halogénées hybrides
A	Cation divalent (Mg^{2+},Ca^{2+},Sr^{2+},Ba^{2+}, …)	Métal alcalin monovalent (Li^{+},Na^{+},K^{+} …)	Petit molécule organique(MA(méthy-lammonium),FA(formamidinium),…)
B	Cation métallique (Ti^{4+},Si^{4+},Sn^{4+}, …)	Métal ionique divalent (Pb^{2+} ou Sn^{2+})	
X	Oxygène	Halogène (Cl^{-},Br^{-} ou I^{-})	

II.4.3. $CsPbI_2Br$ perovskite solar cell

$CsPbI_2Br$ an all-inorganic perovskite material, is considered a promising candidate for solar cells due to its good stability and suitable bandgap. A first principles investigation on the electronic structure, optical properties, and band alignments of $CsPbI_2Br$ reveals the following findings:

- $CsPbI_2Br$ remains stable in a tetragonal cell with a direct bandgap of 1.67 eV, as determined by PBE calculations. The valence band maximum (VBM) is derived from the antibonding states resulting from the hybridization between Pb-s states and halide-p states, while the conduction band minimum (CBM) is primarily composed of Pb-p states.
- $CsPbI_2Br$ exhibits strong optical absorption, with absorption coefficients exceeding 10^4 cm^-1 in the visible light range. This level of absorption is comparable to popular hybrid halide perovskites.
- The band alignments of $CsPbI_2Br$ indicate that commonly used electron transport materials (ETMs) such as TiO2, ZnO, SnO2, PCBM, and C60, as well as hole transport materials (HTMs) such as P3HT, CuI, NiO, PTAA, and Spiro, are suitable for $CsPbI_2Br$ solar cells. The VBM of $CsPbI_2Br$ is higher than that of $CsPbBr_3$ but lower than that of $CsPbI_3$, while the CBM heights are equivalent. This suggests that $CsPbI_2Br$ is more easily doped p-type compared to CsPbBr3 but more challenging than $CsPbI_3$.

In conclusion, $CsPbI_2Br$ possesses desirable electronic and optical properties for solar cell applications. The band alignments indicate compatibility with commonly used ETMs and HTMs, making it a promising material for solar cell technology.

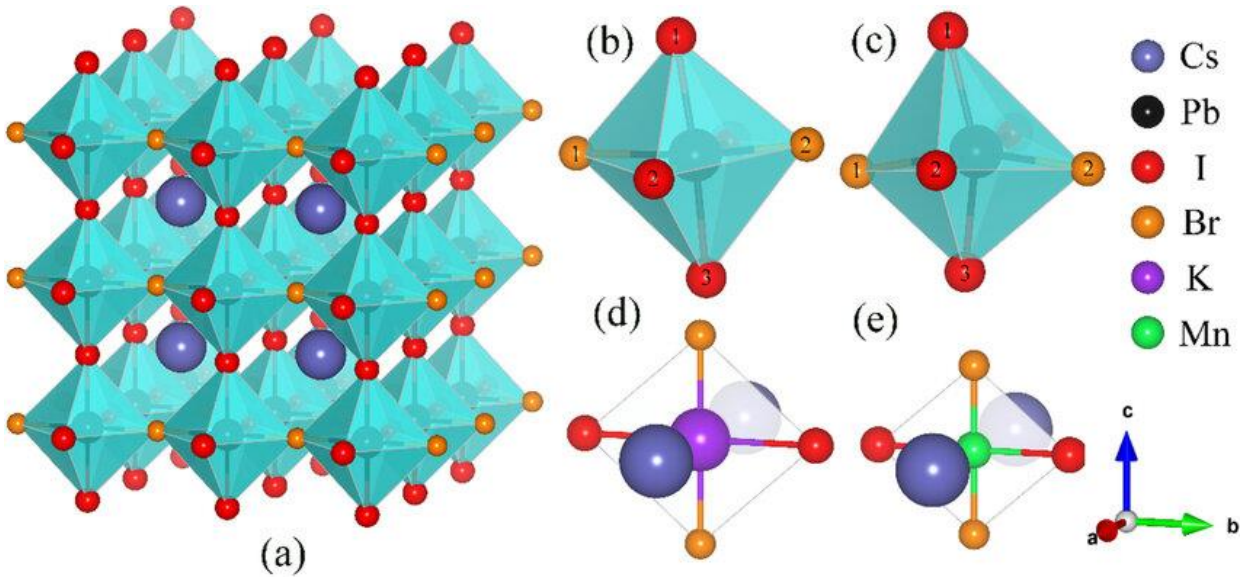

Figure II.15. (a) Lattice structure of undoped $CsPbI_2Br$ supercell, (b), (c) local structures of PbI_4Br_2 octahedrons adjacent to the interstitial K and Mn atoms, (d), (e) local structures of K-and Mn-occupied octahedral interstices.[29]

The lattice structure of $CsPbI_2Br$ consists of corner-sharing octahedra formed by PbI_4Br_2, with Cs atoms at the center of cub-octahedral cavities. The framework of $CsPbI_2Br$ primarily comprises these octahedral units, and changes in the framework structure can be observed through alterations in the Pb-I/Br bond lengths and I-Pb-Br bond angles. The flexibility of the centrally coordinated octahedra of PbI_4Br_2 significantly influences the properties of $CsPbI_2Br$

II.5. Electron Transport Layer (ETL)

The Electron Transport Layer (ETL), also known as Semiconducting Oxide Scaffold or "Couche de Transport d'Électrons" in French, serves as a supporting structure for the sensitizer (perovskite layer) and facilitates electron transfer from the perovskite layer to the FTO.

ETL materials can be classified into three types: organic, inorganic, and polymers. The mesoporous and nanocrystalline structure of the ETL allows efficient charge transport within the perovskite layer. An ideal ETL should have a conduction band that aligns with the perovskite layer's conduction band, promote fast electron transfer while minimizing recombination with the Hole Transport Layer (HTL), and ensure uniform contact with the perovskite materials. Additionally, the ETL should be transparent to maximize the absorption of incident photons by the perovskite layer. Titanium dioxide (TiO_2) is the most commonly used ETL material due to its wide bandgap, which facilitates effective separation of electron-hole pairs and reduces recombination when it possesses a suitable mesoporous morphology. The mesoporous TiO_2 structure, where the pores are filled with perovskite material, has gained popularity and demonstrated higher efficiency in perovskite solar cells. However, other wide-bandgap inorganic oxides such as ZnO, Al_2O_3, SnOx, and organic materials like phenyl-C61-butyric acid methyl ester (PCBM) can also function as ETLs and act as scaffolds in solar cells. Figure II.16 presents a list of several ETL materials used in perovskite solar cell[30].

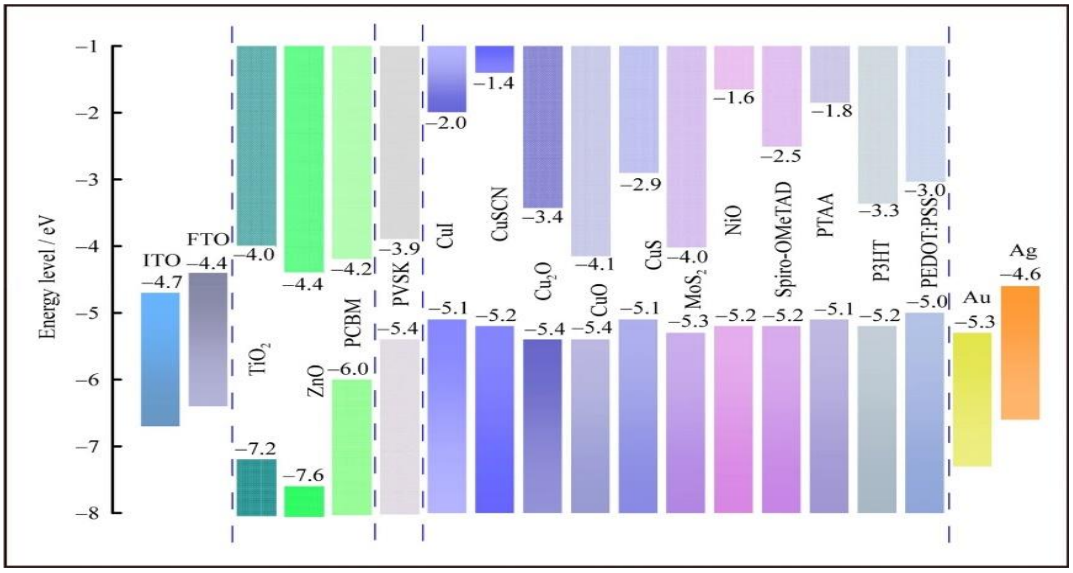

Figure II.16 Energy level diagrams of commonly used materials in perovskite solar cells[31]

II.6. Hole transport layer (HTL)

The Hole Transport Layer (HTL) is used to transport holes from the perovskite layer to the back contact of the conventional solar cell. The HTL is a P-type semiconductor layer that requires high hole mobility (at least $>10^{-4}$ $cm^2V^{-1}s^{-1}$), close alignment with the valence band of the perovskite, good conductivity, and higher stability. Various organic, inorganic, and polymer materials have been explored as HTLs. Figure II.15 depicts the band diagram of HTLs with their highest efficiency in perovskite cells. The most commonly used material for hole transport is spiro-OMeTAD. Spiro-OMeTAD is an amorphous P-type organic semiconductor with a wide bandgap and nearly colorless appearance when deposited as a thin film from a solution onto the substrate. One advantage of spiro-OMeTAD is its ability to fill pores effectively due to its high solubility in toluene and the organic solvent chlorobenzene. However, pristine spiro-OMeTAD has high resistivity and needs to be partially oxidized to improve mobility or doped with P to reduce intrinsic charge transport resistance. Lithium bis(trifluoromethanesulfonyl)imide (LiTFSI) and 4-tert pyridine (tBP) have been used in conjunction with spiro-OMeTAD to enhance conductivity and prevent charge recombination, respectively, in order to achieve better solar cell performance. Perovskite solar cells with polymer HTLs such as poly[bis(4-phenyl) (2,4,6-trimethylphenyl)amine] (PTAA) and poly[3-hexylthiophene-2,5-diyl] (P3HT) exhibit lower stability compared to those with the doped organic HTL, Spiro-OMeTAD, whereas inorganic materials (NiOx and CuSCN) demonstrate greater stability. Therefore, the stability of these organic and polymer materials should be further improved[30]organic and be further improved[30].

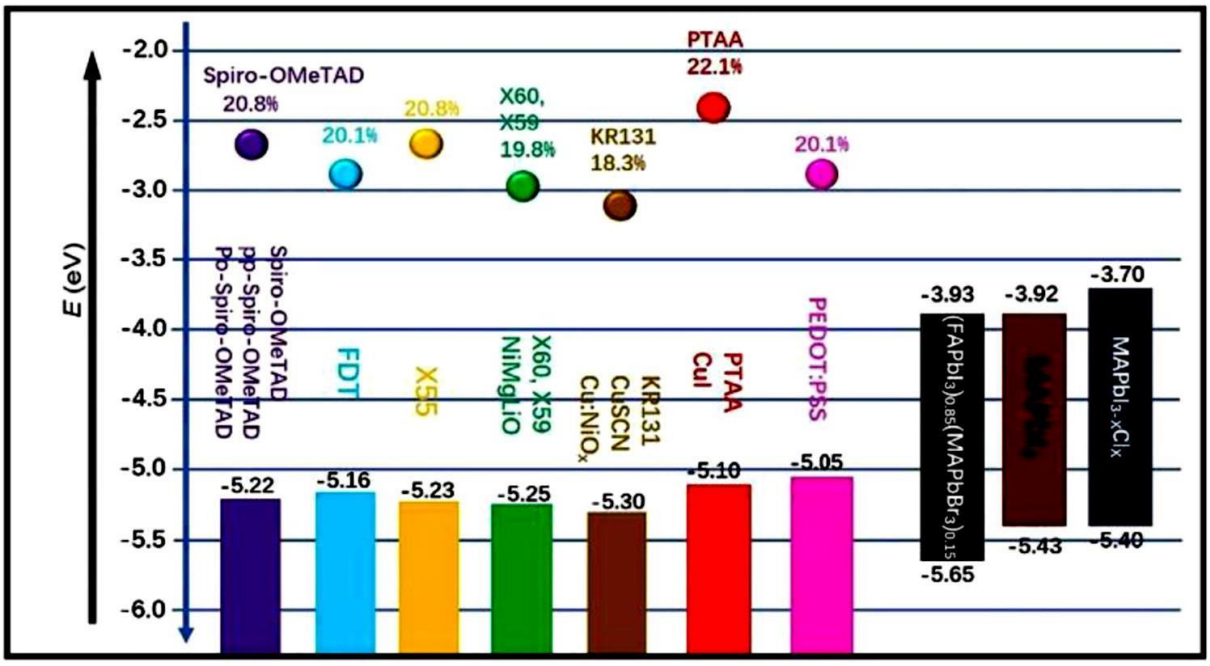

Figure II.17 Energy level diagrams of HTMs (Hole Transport Materials) and PLs (Perovskite Layers) used in perovskite solar cells, including their highest efficiencies.

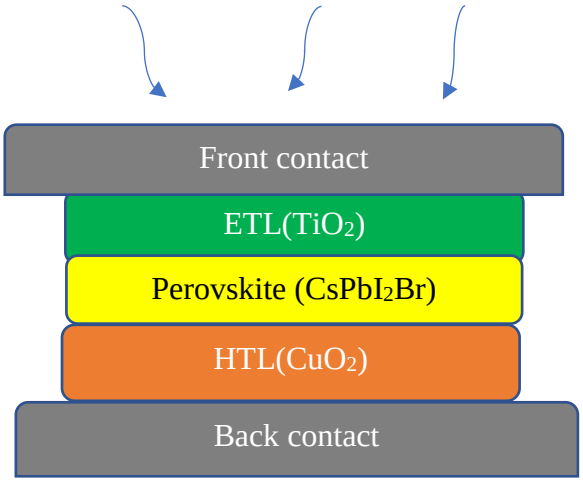

Figure II.18. Schematic structure proposed for perovskite top layer solar cell

II.7. solar cells based on CZTS

Copper, zinc, tin, sulfur, and selenium together form a preferred semiconductor material as it consists of common and non-toxic elements. It is unfortunate that the efficiency displayed by CZTS cells is not higher, but it is expected to increase in the coming years. Will CIGS and CdTe soon have a top-notch replacement? New cells are already being developed in anticipation of the likely indium shortage. However, replacing CIGS cells poses a real challenge due to their efficient absorber. Nonetheless, an alternative based on the p-n junction principle has emerged since the late 2000s: the CZTS cell.

Copper-zinc-tin-sulfur (CZTS) is a semiconductor with excellent photovoltaic properties, such as a direct bandgap and a high absorption coefficient. It possesses an optimal band energy of 1.4 to 1.5 eV, which is highly desirable for photovoltaic applications. Furthermore, CZTS cells utilize abundant (non-rare) and non-toxic materials, resulting in low production costs. The availability of copper, zinc, tin, and sulfur in the Earth's crust is approximately 50 ppm, 75 ppm, 2.2 ppm, and 260 ppm, respectively. In contrast, the availability of indium is relatively very low at 0.049 ppm, making it[10] scarce compared to zinc and tin[32].

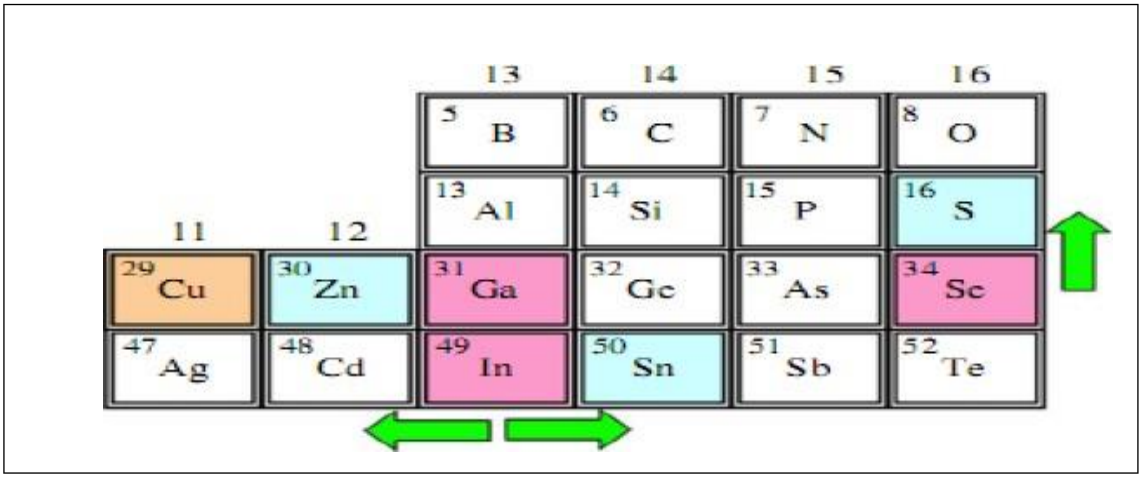

Figure II.19. The section of the periodic table showing the logic of the evolution from CIGS to CZTS involves the transition from Group 12 to Group 14.

If there are no rare earth elements or toxic substances, what is used instead? CZTS solar cells actually contain an absorber made of copper, zinc, tin, sulfur, and selenium, with the chemical formula $Cu2ZnSn(S,Se)_4$. The addition of another n-doped semiconductor is required

to form a heterojunction, similar to CIGS cells. According to an article published in 2009, it is estimated that we could produce enough energy to meet the needs of the global population by utilizing only 0.1% of the reserves of the key elements involved.

II.7.1. CZTS Properties

CZTS, a semiconductor material used in solar cells, can be obtained by replacing half of the indium atoms in the chalcopyrite CuInS2 with zinc and the other half with tin. This substitution is preferred for the production of low-cost solar cells. When forming a heterojunction with CZTS, CdS needs to be replaced by zinc sulfide (ZnS) as it provides the desired bandgap.

According to Shockley-Queisser photon balance calculations, CZTS is expected to have a theoretical efficiency of over ~30% [33]. The highest efficiency is achieved in CZTS solar cells with low copper content and high zinc content, as this favors the growth of other phases during film formation [34]. Due to the low proportion of zinc and high proportion of copper, the CZTS layer becomes more of a p-type semiconductor[35]. Depicts the schematic diagram of a thin-film CZTS solar cell.

CZTS is derived from the structure of CIGS by iso-electronic substitution of two indium (or gallium) atoms with one zinc atom and one tin atom. As a result, CZTS exhibits similar properties to the CIGS layer. One major advantage of this device is that it can adopt the standard structure of solar cells. The crystal structure of CZTS, known as kesterite, is represented in Figure II.4. It can be obtained by duplicating the unit cell of the sphalerite structure. The kesterite structure is the most stable phase of CZTS.

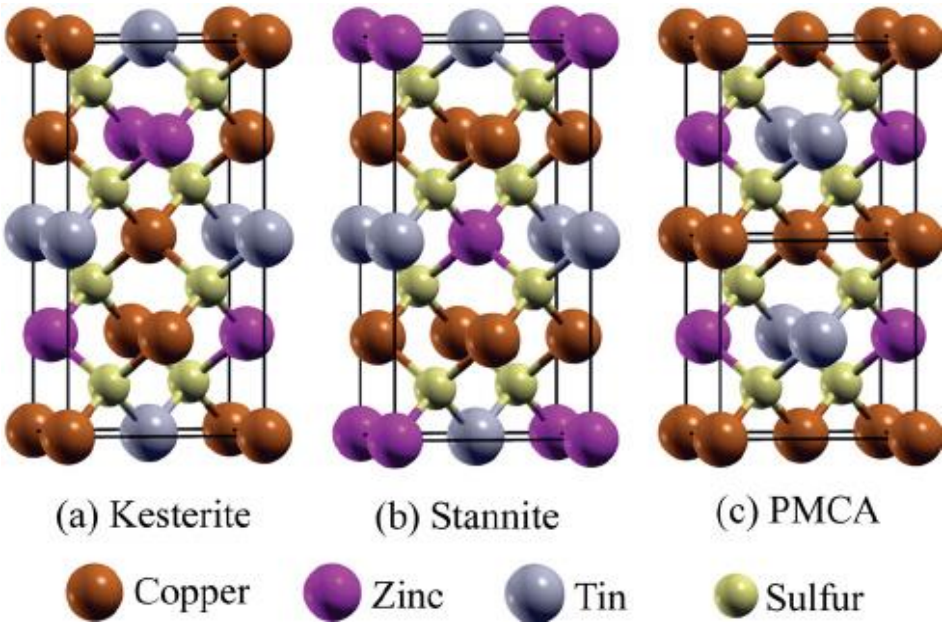

Figure II.20. Kesterite structure in which CZTS crystallizes. It is derived from the sphalerite structure by duplicating the unit cell [36].

CZTS (Cu_2ZnSnS_4) is closely related to CIGS, Essentially, the expensive and scarce elements of indium and gallium are replaced by a 50:50 combination of much cheaper zinc and tin. At the same time, selenium (Se) is replaced by sulfur (S) due to the bandgap of Cu2ZnSnS4 (1.45 eV), which is closer to the optimal value for the corresponding selenide compound with a narrower bandgap. All cations are ordered in the kesterite structure.

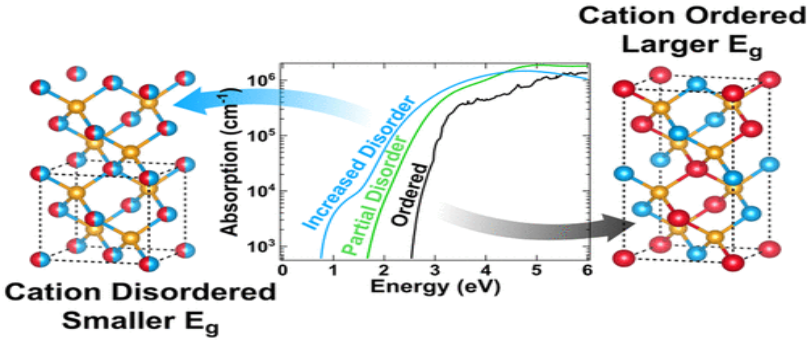

Figure II.21. The special quasi-random structure of Cu2ZnSn(S:Se)$_4$ with cations ordered in the kesterite structure [37].

II.7.2. CZTS/P-Si: Advancing Solar Cell Efficiency

Numerous studies have investigated the P-CdS/P-CZTS/P-Si heterojunction architecture in the field of photovoltaics, highlighting its potential for high-performance solar cells. In these studies, researchers have focused on optimizing the individual layers and the overall device structure to enhance the efficiency, stability, and scalability of the solar cells.

Starting with the P-CdS window layer, it has been extensively studied as a means to improve light transmission and reduce surface recombination losses. By carefully controlling the thickness and doping of the P-CdS layer, researchers have achieved higher light absorption and improved charge carrier collection at the interface. Various deposition techniques, such as chemical bath deposition and physical vapor deposition, have been employed to fabricate high-quality P-CdS films with controlled properties.

Moving on to the P-CZTS absorber layer, it offers several advantages over other thin film materials, particularly in terms of abundance, non-toxicity, and cost-effectiveness. The composition of copper, zinc, tin, and sulfur can be optimized to achieve the desired bandgap and electronic properties for efficient solar energy conversion. Researchers have explored different synthesis methods, including solution-based processes, sputtering, and co-evaporation, to obtain high-quality P-CZTS films with suitable crystalline structure and composition control.

The P-Si substrate, which serves as the foundation for the heterojunction structure, offers excellent electronic properties and compatibility with conventional silicon-based solar cell technologies. Its established manufacturing processes and well-understood characteristics provide a robust platform for integrating the P-CdS/P-CZTS layers. Researchers have focused on surface passivation techniques and interface engineering to minimize carrier recombination at the P-Si/P-CdS and P-CZTS/P-Si interfaces, leading to improved device performance.

To further enhance the efficiency and stability of the P-CdS/P-CZTS/P-Si solar cells, researchers have investigated additional strategies, such as interface buffer layers, antireflection coatings, and device encapsulation[43] .These approaches aim to optimize light trapping, reduce optical losses, and protect the device from environmental degradation.

The ultimate goal of these studies is to contribute to the development of sustainable and cost-effective solar cell technologies. By improving the efficiency and scalability of the P-CdS/P-CZTS/P-Si heterojunction architecture, researchers hope to accelerate the adoption of solar energy as a viable and environmentally friendly power source. Continued research efforts and technological advancements in this field hold the potential to revolutionize the renewable energy landscape and contribute to a greener and more sustainable future.

II.8. Conclusion

In conclusion, SCAPS 1-D software has proven to be a valuable tool in the field of photovoltaics, enabling researchers to simulate and optimize the performance of solar cells. It allows for the investigation of various parameters, such as layer thicknesses and material properties, to improve device efficiency and performance.

Perovskite materials, including $CsPbI_2Br$, have emerged as promising candidates for next-generation solar cells due to their unique optoelectronic properties. However, challenges related to stability and scalability need to be addressed for their commercialization.

In perovskite solar cells, the choice of hole transport layers (HTL) and electron transport layers (ETL) plays a critical role in facilitating efficient charge transport and reducing recombination losses. Suitable HTL and ETL materials and their proper engineering are essential for achieving high device performance.

Furthermore, the integration of CZTS (Cu_2ZnSnS_4) with silicon in a heterojunction architecture holds promise for cost-effective and environmentally friendly solar cells. CZTS/Si heterojunctions benefit from the complementary properties of CZTS and silicon, offering enhanced light absorption and efficient charge carrier extraction.

Ongoing research is focused on improving the stability, scalability, and overall performance of perovskite solar cells and CZTS/Si heterojunctions. Through advancements in material formulations, device architectures, and interface engineering, researchers aim to accelerate the development of efficient and sustainable photovoltaic technologies for a clean energy future.

CHAPTER III

ANALYSIS & RESULT WITH DISCUSSION

III.1. Introduction

In this chapter, our focus is on studying and simulating a tandem solar cell consisting of two layers. The top layer comprises an inorganic perovskite material, specifically a structure of CuO_2/$CsPbI_2Br$/TiO_2.

The bottom layer consists of a combination of materials including p-Si, p-CZTS, n-CdS, i-ZnO, and Al-ZnO. To conduct our simulations, we will utilize the numerical simulation software SCAPS.

Our approach begins by studying the bottom layer independently, without the top layer. We will investigate various factors such as thicknesses, band gaps, and doping levels for CZTS and CdS.

By carefully analyzing these parameters, we aim to identify the optimum conditions that yield the best performance for the bottom layer. Subsequently, we will examine the tandem solar cell as a whole using the contour profile method.

This analysis allows us to evaluate the overall performance and efficiency of the tandem structure. Through this comprehensive study, we intend to gain valuable insights and optimize the design of the tandem solar cell.

III.2 Study of the structure of the Bottom solar cell (without Perovskite)

The lowermost layer of our solar cell is constructed with a precise arrangement of multiple materials, each serving a specific purpose.

The first layer, known as p-Si, consists of silicon that has been positively doped, meaning it has an abundance of positively charged carriers. This layer sets the foundation for the subsequent layers.

Above the p-Si layer is the p-CZTS layer, which stands for copper zinc tin sulfide. This layer is also positively doped, meaning it contains an excess of positive charge carriers. The addition of copper, zinc, and tin to the sulfide material enhances its ability to absorb light effectively.

Following the p-CZTS layer is the n-CdS layer, where the 'n' stands for negatively doped. In this layer, cadmium sulfide is doped with negatively charged carriers, resulting in an excess of negative charge carriers. The n-CdS layer serves as a bridge between the p-CZTS layer and the subsequent layers, facilitating the flow of electrons.

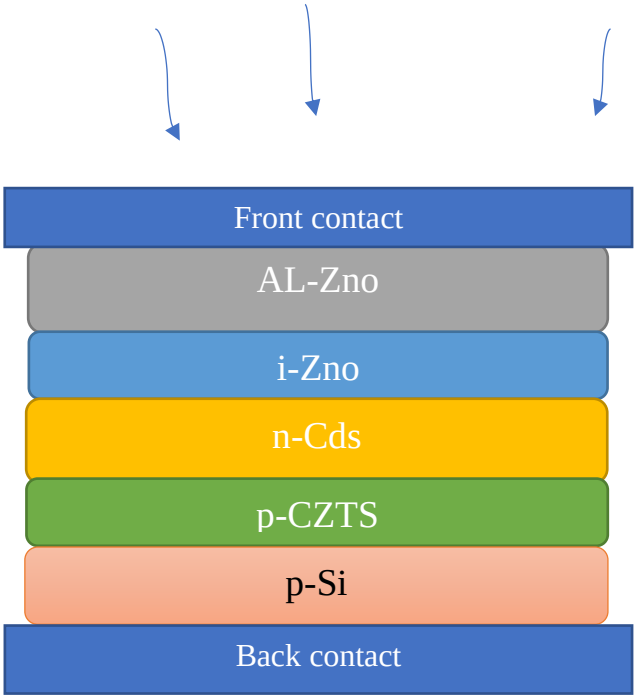

Figure III.1. Schematic structure proposed bilayer CZTS/Si absorber solar cell

Next in line is the i-ZnO layer, which stands for undoped zinc oxide. This layer is not intentionally doped with any charge carriers, allowing it to function as a semi-conductor with intrinsic properties. The i-ZnO layer plays a crucial role in absorbing light and generating electron-hole pairs within the solar cell [

Finally, the Al-ZnO layer, or aluminum-doped zinc oxide layer, is added as the topmost layer of the bottom section. This layer incorporates aluminum atoms into the zinc oxide structure, which helps to optimize the electrical conductivity of the cell and improve its overall performance[44].

By carefully arranging these layers, the solar cell is designed to efficiently absorb incoming sunlight and convert it into charge carriers, which can be harnessed as electrical energy. Each layer contributes to this process by creating favorable conditions for light

absorption and charge carrier generation, ultimately enhancing the overall efficiency of the solar cell.

Table III.1: The material parameters of bottom layers used in SCAPS-1D[38]

Properties	Si	CZTS	CdS	i-ZnO	AZO
Thickness (nm)	Variable	variable	50	100	150
Bandgap E_g (Ev)	1.12	1.450	2.600	3.370	3.370
Elec. Aff χ(eV)	4.05	4.100	3.750	4	4
Dielc.per ϵ_r(relative)	11.68	7	8.730	9	9
DOS. CB (cm-^{3})	$2.82x10^{19}$	$2.2x10^{18}$	$3.3x10^{18}$	$3.6x10^{18}$	$3.6x10^{18}$
DOS. VB (cm^{-3})	$1.83x10^{19}$	$7x10^{*19}$	$1.36x10^{19}$	$1.13x10^{19}$	$1.13x10^{19}$
Electron thermal velocity (cm/s)	$1x10^7$	$1x10^7$	$1x10^7$	$1x10^7$	$1x10^7$
Hole thermal velocity (cm/s)	$1x10^7$	$1x10^7$	$1x10^7$	$1x10^7$	$1x10^7$
Electron mobility (cm^2/Vs)	1100	100	160	150	150
Hole mobility (cm^2/Vs)	420	35	15	50	50
Donor density N_D (cm^{-3})	-	-	$1x10^{17}$	-	$8x10^{18}$
acceptor density, N_A (cm^{-3})	variable	variable	-	-	-
Defect type (cm^{-3})	Neutral variable	Neutral variable	$1x10^{15}$	$1x10^{16}$	$1x10^{16}$

Table III.2 : The bottom layer defect used in SCAPS-1D[38]

Properties	Defect type	Total Density (N_t)	Capture cross section electrons (cm^2)	Capture cross section holes (cm^2)	Energetic distribution	Energy level with respect to reference
p-SI	scaps model	scaps model	scaps model	scaps model	scaps model	scaps model
p-CZTS	Donor	1.00E+14	5.00E-13	1.00E-15	single	0.1-0.4 ev
	Acceptor	5.00E+14	1.00E-15	1.00E-15	single	0.5-0.3ev
n-CdS	scaps model	scaps model	scaps model	scaps model	scaps model	scaps model
n-ZnO	scaps model	scaps model	scaps model	scaps model	scaps model	scaps model
CZTS/CdS	Neutral	1.00E+12	1.00E-14	1.00E-14	uniform	0.6

TABLE III. 3: The material parameters of top layers used in SCAPS-1D[39]

Properties	TiO_2(ETL)	$CsPbI_2Br$	CuO_2(HTL)
Thickness(um)	0.04	1	0.250
Bandgap(eV)	3.2	1.5	2.170
Affinity(eV)	3.9	3.7	3.200
Dielec. Perm	9	8.6	7.11
DOS CB(cm^{-3})	$1x10^{21}$	$1.9x10^{19}$	$2.02x10^{17}$
DOS VB(cm^{-3})	$2x10^{20}$	$2.37x10^{20}$	$1.1x10^{19}$
µe(cm2/Vs)	20	25	200
µh(cm2/Vs)	10	25	80
Donor.Con.(cm^{-3}) Nd	$2x10^{-19}$	-	-
Accep.Con.(cm^{-3}) Na	-	$1x10^{15}$	$1x10^{18}$
Absoption	-	scaps model	scaps model
Nt defect (cm^{-3})	$3.6x10^{16}$	$1x10^{17}$	$1x10^{17}$

III.2.1. Study of different effect (bottom layer)

In our study, we have investigated the effects of varying the thickness, doping level, and band gap of the CZTS material. The remaining parameters have been kept constant, as outlined in the table.

III.2.2. Effect of CZTS thickness (bottom layer)

Figure III.2. Effect of CZTS thickness variation

a)

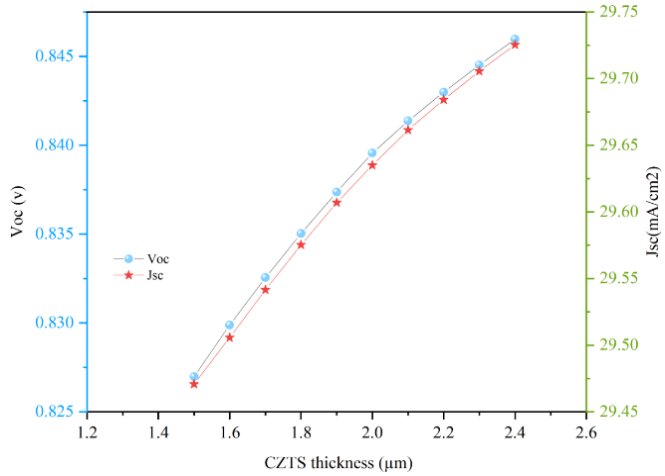

b)

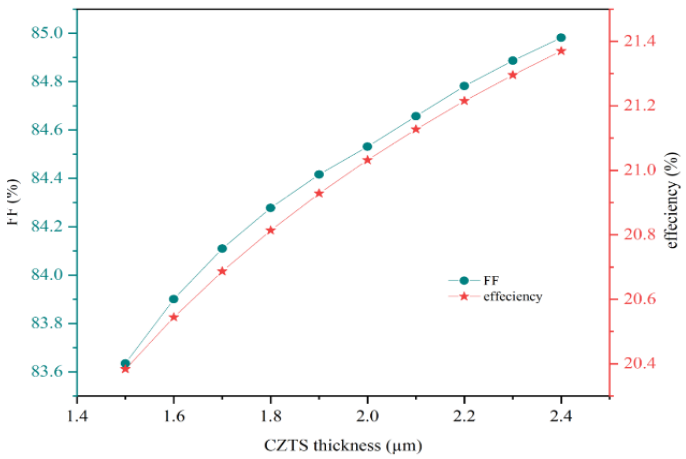

c)

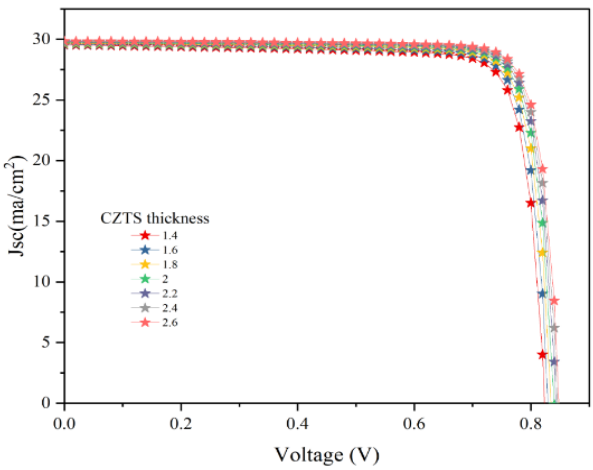

d)

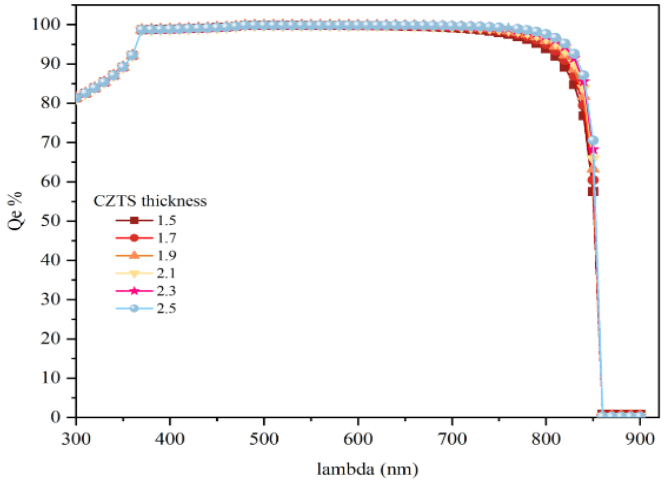

In Figure 2(a), it is evident that with an increase in the thickness of the p-CZTS layer, both the short-circuit current (Jsc) and open-circuit voltage (Voc) exhibit a noticeable upward trend. This behavior signifies a greater absorption of incident light, leading to the generation of a higher number of electron-hole pairs. Consequently, the Jsc is enhanced due to the augmented population of charge carriers. Moreover, the increased thickness of the p-CZTS layer contributes to a reduction in the likelihood of recombination events. This is because the larger volume of charge carriers allows for more opportunities for diffusion without encountering recombination. Consequently, the open-circuit voltage (Voc) experiences an elevation.

The combination of increased Jsc and Voc contributes to a higher fill factor (FF) and overall improved efficiency, as clearly demonstrated in Figure 1(b) and 1(c). These factors collectively result in a higher quantum efficiency (QE), indicating the enhanced ability of the solar cell to convert incident photons into electrical current.

In summary, the experimental findings in Figure 1 highlight that increasing the thickness of the p-CZTS layer in the solar cell leads to several favorable outcomes, including enhanced light absorption, increased population of charge carriers, reduced recombination, elevated open-circuit voltage, improved fill factor, and ultimately, higher quantum efficiency.

The combination of increased Jsc and Voc contributes to a higher fill factor (FF) and overall improved efficiency, as clearly demonstrated in Figure 2(b) and 2(c). These factors collectively result in a higher quantum efficiency (QE), indicating the enhanced ability of the solar cell to convert incident photons into electrical current.

III.2.3. Effect of CZTS dopage (bottom layer)

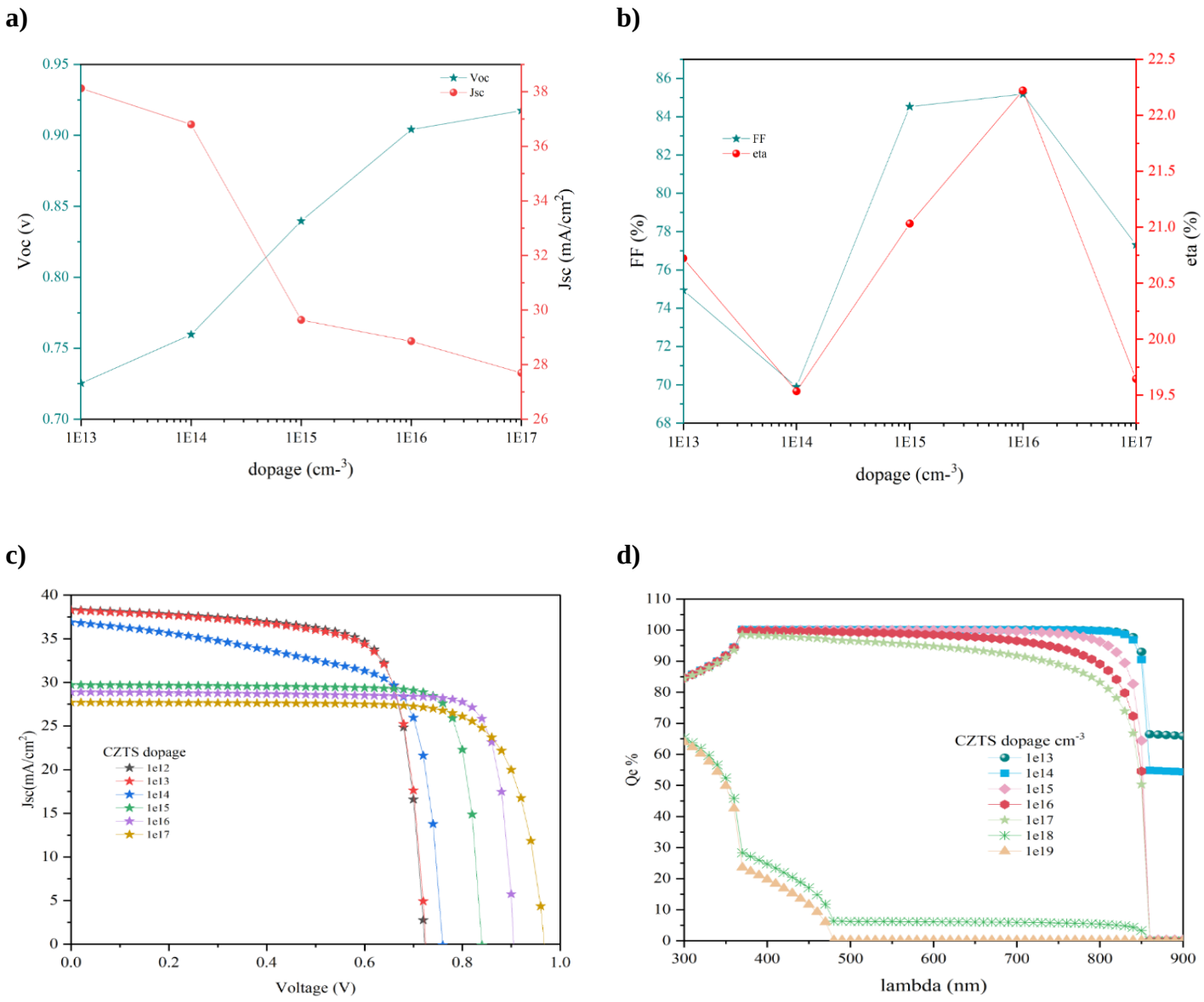

Figure III.3. Effect of CZTS dopage variation

In Figure 3(a), the analysis reveals that increasing doping concentration also leads to an increase in defect density. This means that a higher concentration of dopants results in a greater density of defects within the material. These defects can act as centers for charge carriers and

significantly increase the probability of recombination occurring. As a consequence, there is a decrease in the short-circuit current (Jsc) at a certain level of doping concentration.

However, the situation is quite different for the open-circuit voltage (Voc). Higher doping concentrations have the potential to modify the transport properties of charge carriers, such as the diffusion length, and can also impact the presence of certain defects. These modifications can enhance the extraction and collection of charge carriers at the electrode interface, resulting in a higher Voc.

However, as the doping concentration further increases from 1e14 cm^{-3} to 1e17 cm^{-3}, there is a notable improvement in both FF and efficiency. This behavior can be explained by the modification of transport properties and the impact on specific defects that occur with higher doping concentrations. The increased doping concentration can enhance the transport characteristics of charge carriers, such as the diffusion length, enabling more efficient extraction and collection of charge carriers at the electrode interface. This improvement in charge carrier transport contributes to higher FF values. Additionally, the higher doping concentration may also affect the presence or characteristics of certain defects, potentially reducing their detrimental impact on recombination. This further enhances the performance of the solar cell, leading to an increase in efficiency.

III.2.4. Effect of CZTS band gap (bottom layer)

a)

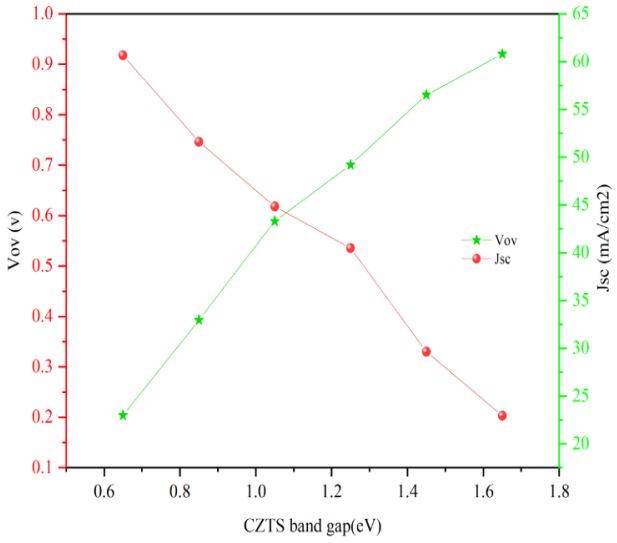

b)

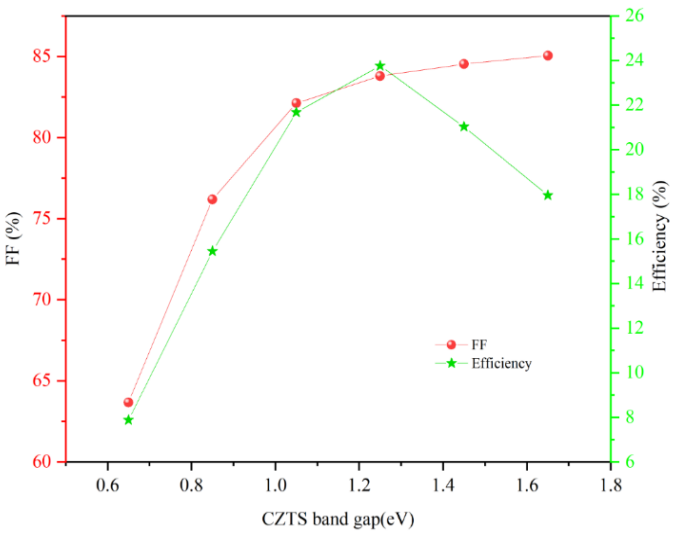

c)

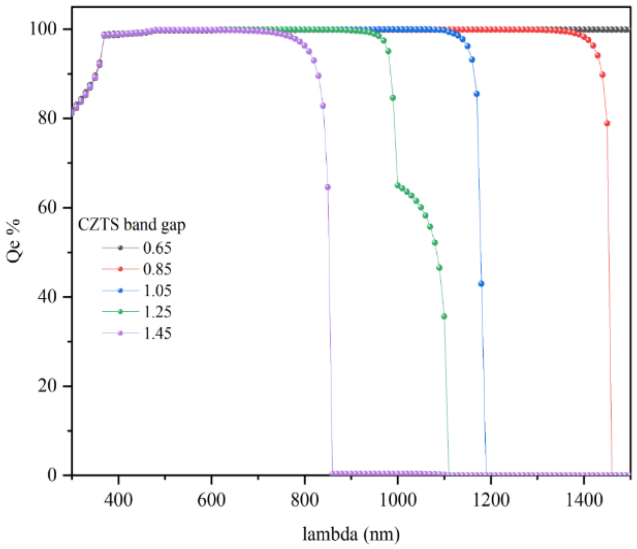

d)

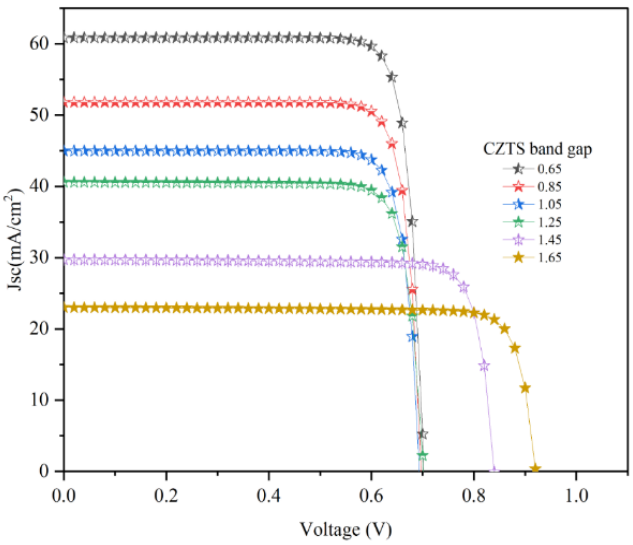

Figure III.4. Effect of CZTS band gap variation

In the given figure, it is evident that a larger band gap in CZTS (Copper Zinc Tin Sulfide) leads to a higher potential and increased open-circuit voltage (Voc). This is because the larger band gap creates a higher energy barrier, preventing charge carriers from passing through easily. As a result, the charge carriers experience enhanced separation and reduced recombination, leading to a higher Voc.

On the other hand, for the short-circuit current (Jsc), the situation is opposite. A smaller band gap allows for a wider range of photon energies to be absorbed, including a larger portion of the solar spectrum. Consequently, more photons are absorbed, resulting in a higher Jsc, as depicted in Figure 4(a).

However, it is important to note that there exists an optimal range for the band gap that maximizes the fill factor (FF) and efficiency. This optimal range ensures a balance between the absorption of photons and the prevention of recombination, leading to improved FF and overall efficiency, as shown in Figures 4(b) and 4(c).

III.2.5. Effect of CdS thickness (bottom layer)

Regarding the open-circuit voltage (Voc), the thickness of the CdS layer plays a role in minimizing recombination losses. A thicker CdS layer can act as a better barrier against the recombination of charge carriers, leading to a higher Voc. The CdS layer effectively blocks the recombination of electrons and holes at the interface between the CdS and the absorber layer, allowing for efficient charge separation and an increase in Voc.

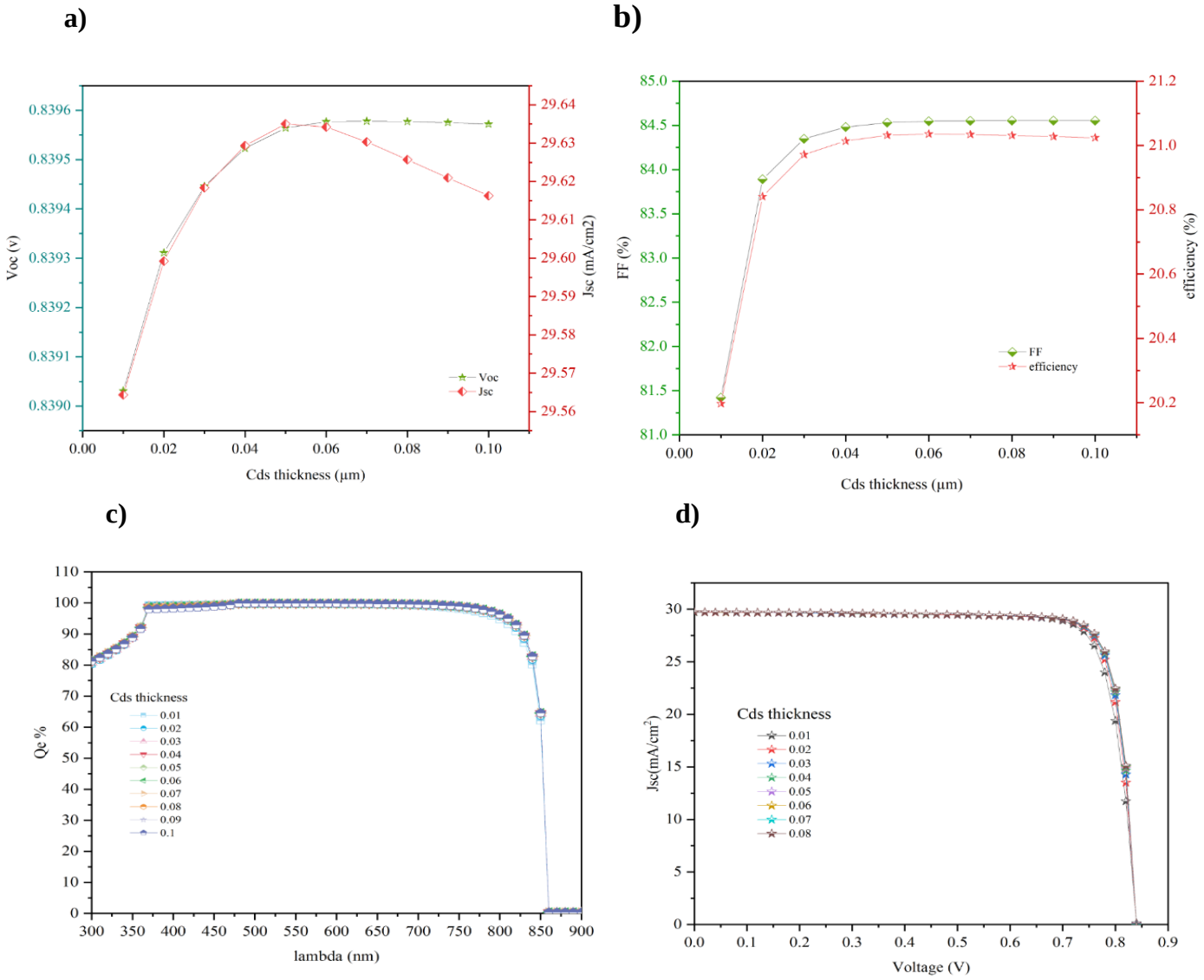

Figure III.5. the effect of CdS thickness variation

However, there is an optimal thickness for the CdS layer that maximizes the device performance. If the CdS layer becomes too thick, it may absorb a significant amount of light,

reducing the current reaching the absorber layer and decreasing the overall efficiency of the solar cell.

Therefore, finding the right balance in CdS layer thickness is crucial to optimize the Voc and overall performance of the solar cell. Researchers and engineers carefully optimize the CdS layer thickness to achieve the desired trade-off between charge carrier separation and light absorption, ultimately maximizing the efficiency of CdS-based thin-film solar cells.

III.2.6. Effect of CdS band gap (bottom layer)

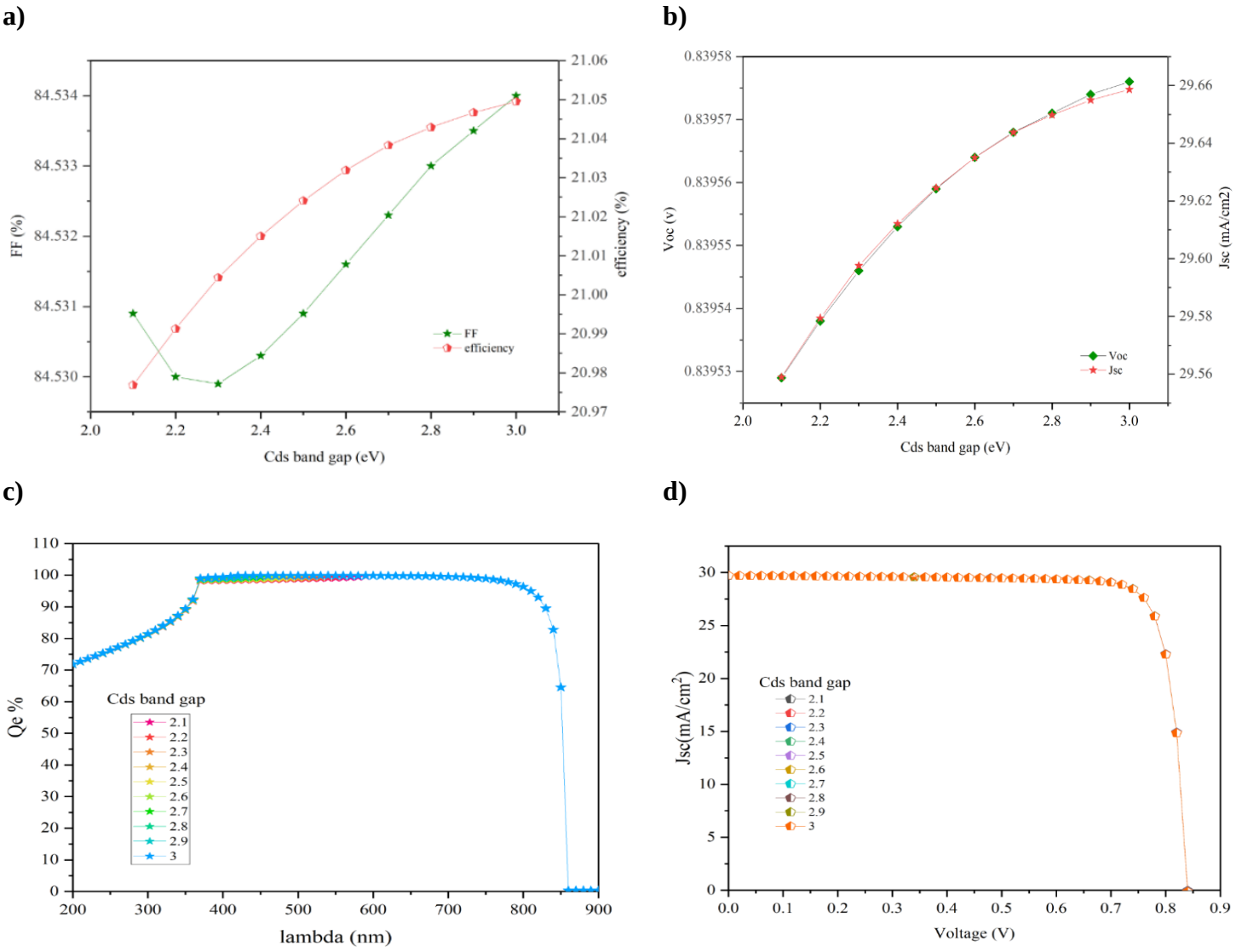

Figure III.6. Effect of CZTS band gap variation

Figure 6(b) demonstrates that increasing the band gap of CdS from 2.1 eV to 3 eV has a minimal impact on the open-circuit voltage (Voc) of the solar cell. This effect is primarily attributed to the built-in potential generated at the interface between CdS and CZTS. The alignment of energy levels at this interface is influenced by the band gap of CdS, resulting in a slight increase in Voc.

III.2.7. Effect of CdS dopage (bottom layer)

a) b)

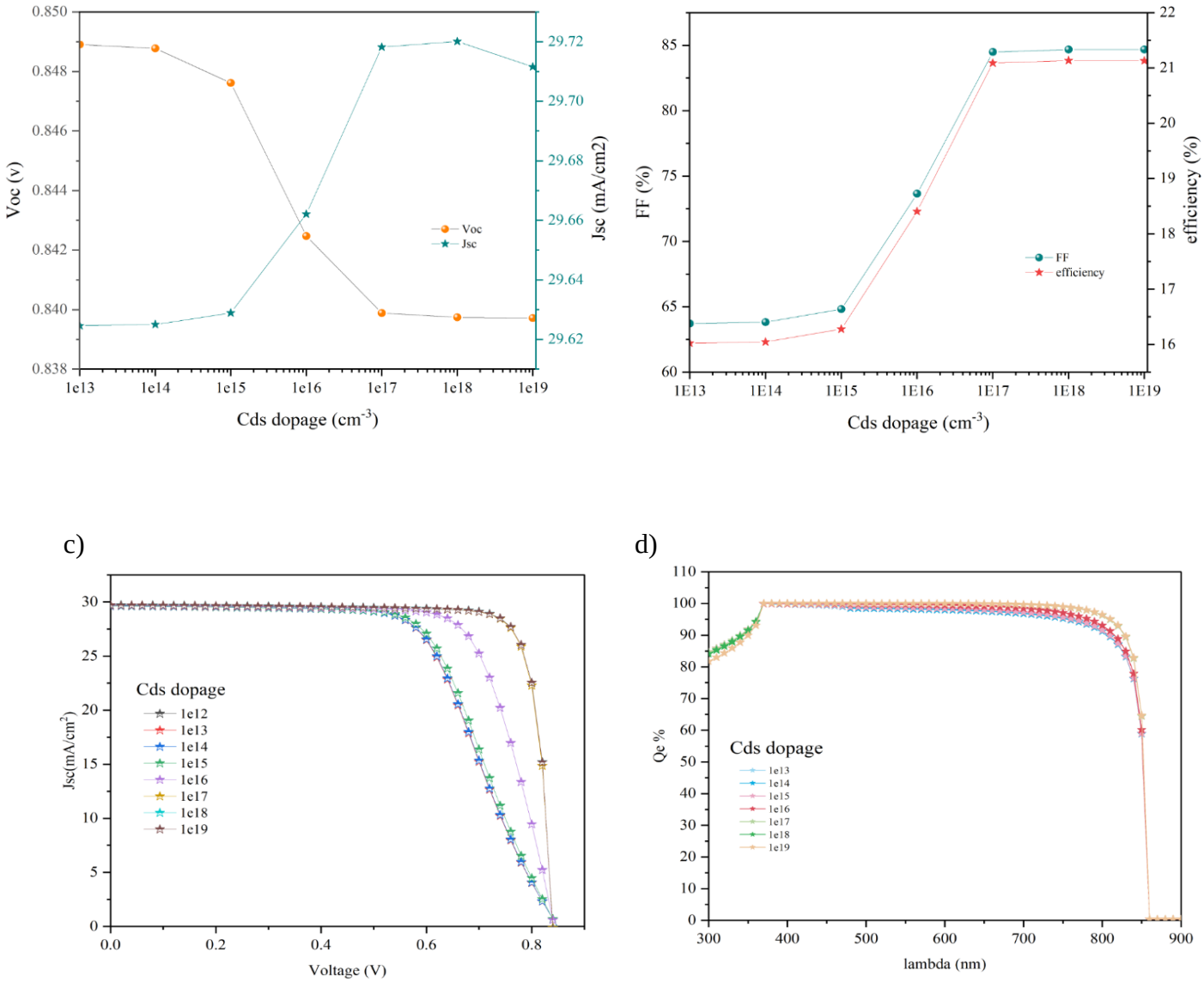

Figure III.7. the effect of CdS dopage variation

In Figure 7(b), it is observed that the doping concentration of CdS has an optimal range from 1E15 cm^{-3} to 1E17 cm^{-3}. Within this specific range, the doping concentration has a significant impact on the electrical and optical properties of the material. The optimal doping concentration leads to improved conductivity, which in turn may result in higher charge carrier mobility. This increased mobility contributes to higher short-circuit current (Jsc) values. Similarly, for the open-circuit voltage (Voc), the slight reduction observed is mainly attributed to energy level alignment at the n-CdS/p-CZTS interfaces, but this effect is negligible.

The findings from Figure 7(b) are further supported by Figure 7(a), which shows that higher doping concentrations effectively reduce recombination rates by passivating trap states. This reduction in recombination leads to an improvement in the fill factor (FF) and overall efficiency. Consequently, the global current level in the I-V curve increases with higher CdS doping concentrations, up to a certain level.

optimal CdS doping concentrations within the specified range enhance the electrical and optical properties of the material, resulting in improved charge carrier mobility, reduced recombination rates, higher Jsc and Voc values, and enhanced FF and efficiency in the solar cell.

III.3. Study of the structure on tandem solar cell (with Perovskite)

In this section, we will employ an in-depth analysis using a contour profile approach to thoroughly investigate and understand the intricate effects of manipulating the thickness and band gap of the tandem solar cell. Our objective is to gain comprehensive insights into how changes in these parameters impact the overall efficiency and performance of the solar cell structure, specifically focusing on the top layer composed of CuO_2 as the hole transport layer (HTL), $CsPbI_2Br$ as the active layer, and TiO_2 as the electron transport layer (ETL).

By meticulously studying the contour profiles, we aim to unravel the complex interplay between thickness, band gap, and their subsequent influence on the electrical characteristics of the tandem solar cell. This meticulous examination will shed light on the intricate relationships and trade-offs associated with these parameters, enabling us to unravel the optimal configuration for enhanced efficiency and performance.

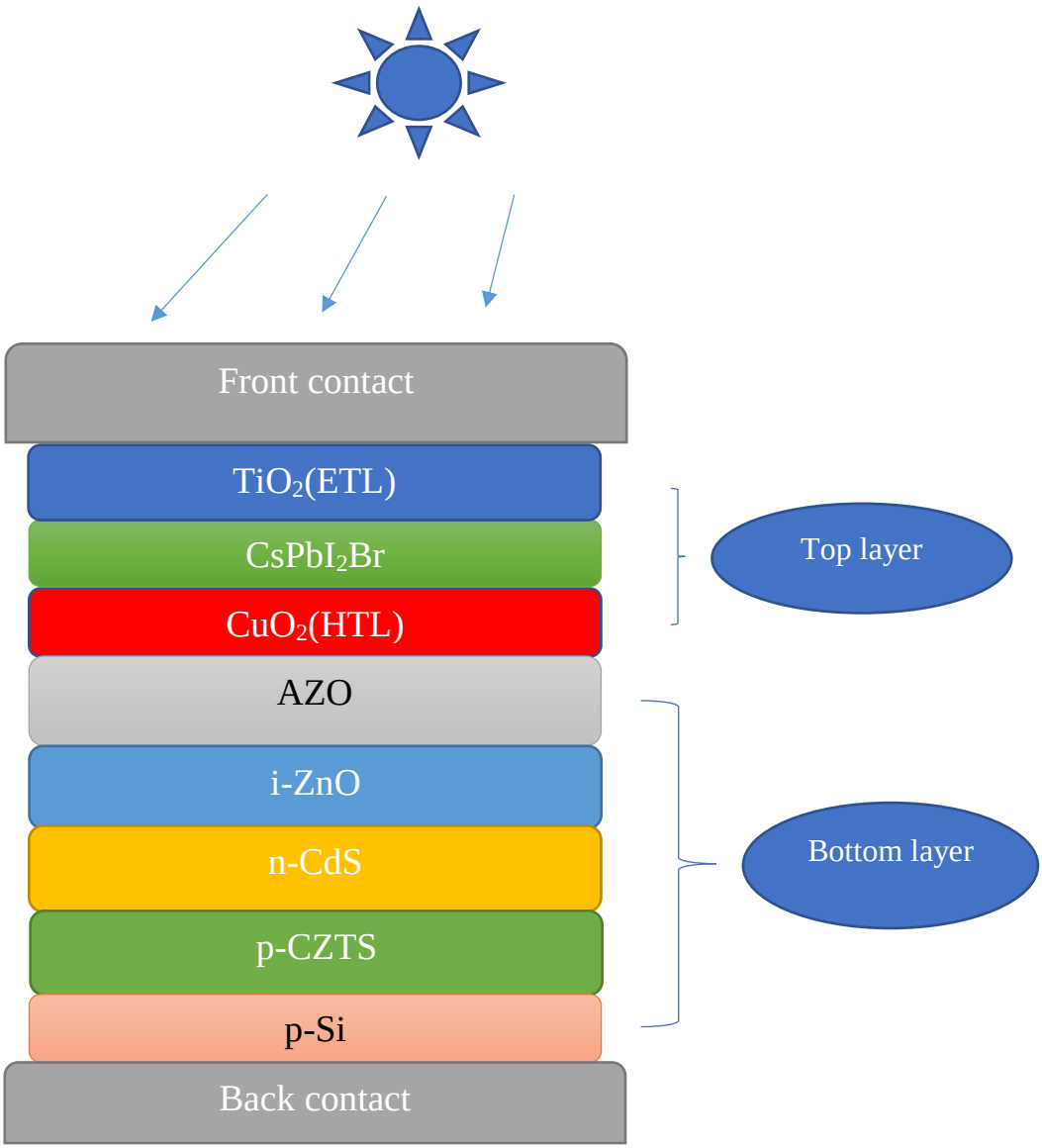

Figure III.8 . Schematic structure proposed for a tandem solar cell

II.3.1. Effect of thickness on CZTS and perovskite (tandem solar cell

Heat map profile: A heat map is a two-dimensional representation of data in which values are represented by colors. A simple heat map provides an immediate visual summary of information. More elaborate heat maps allow the viewer to understand complex data sets. There can be many ways to display heat maps, but they all share one thing in common, they use color to communicate relationships between data values that would be much harder to understand if presented numerically in a spreadsheet . [40]

A contour plot: is a graphical technique for representing a 3-dimensional surface by plotting constant z slices, called contours, on a 2-dimensional format. That is, given a value for z, lines are drawn for connecting the (x,y) coordinates where that z value occurs.[41]

a) b)

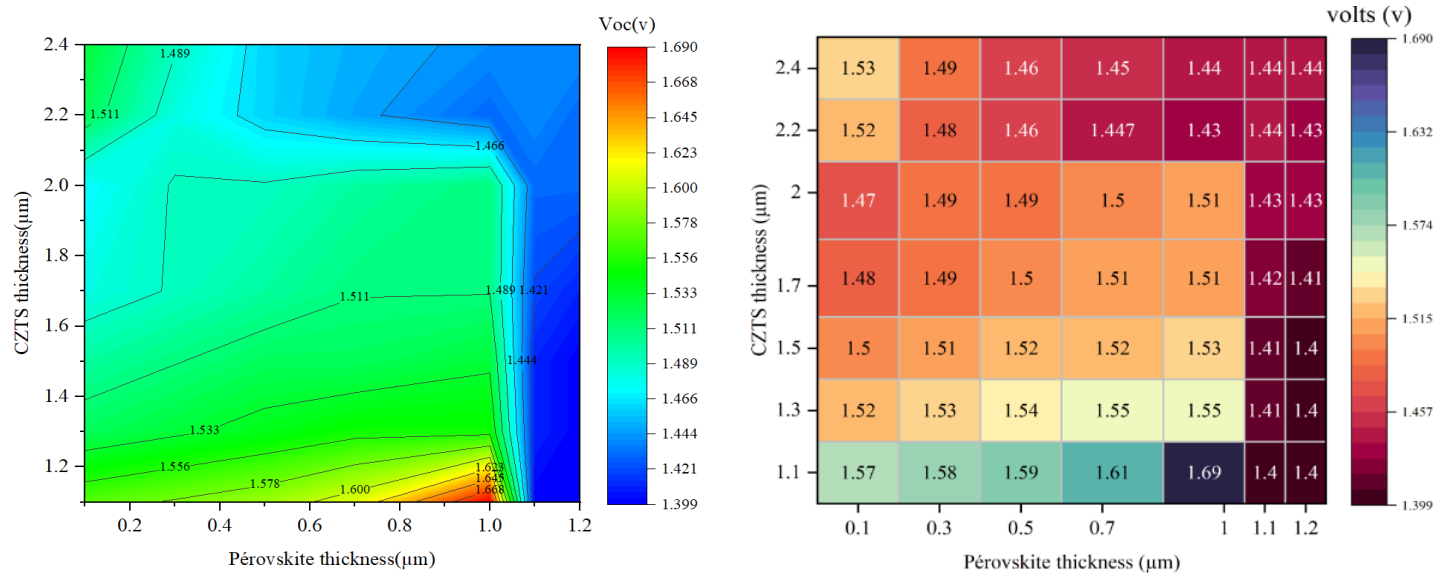

Figure III.9. Effect of thickness on tandem solar cell in Voc

By progressively increasing the thickness of both the copper zinc tin sulfide (CZTS) and perovskite layers within the tandem solar cell, we observe an initial rise in the short-circuit current (Jsc), as visually represented by the varying colors in the contour profile figure. The gradient from red to blue indicates improved to diminished performance, respectively. The rationale behind this trend lies in the thicker CZTS and perovskite layers enabling enhanced absorption of a wider range of photon energies. Consequently, a higher number of electron-hole pairs are generated, leading to an increase in Jsc.

c.1)

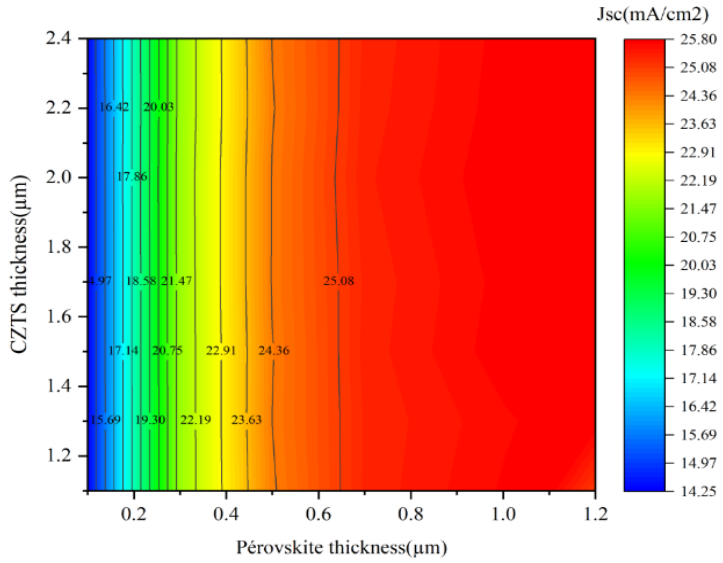
Jsc(mA/cm2)
CZTS thickness(µm)
Pérovskite thickness(µm)
16.42
20.03
17.86
14.97
18.58
21.47
25.08
17.14
20.75
22.91
24.36
15.69
19.30
22.19
23.63

d.1)

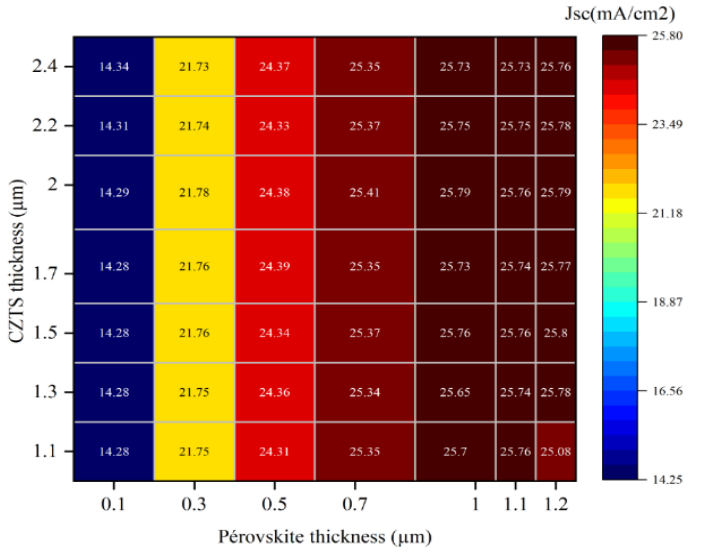
Jsc(mA/cm2)
CZTS thickness (µm)
Pérovskite thickness (µm)
14.34 21.73 24.37 25.35 25.73 25.73 25.76
14.31 21.74 24.33 25.37 25.75 25.75 25.78
14.29 21.78 24.38 25.41 25.79 25.76 25.79
14.28 21.76 24.39 25.35 25.73 25.74 25.77
14.28 21.76 24.34 25.37 25.76 25.76 25.8
14.28 21.75 24.36 25.34 25.65 25.74 25.78
14.28 21.75 24.31 25.35 25.7 25.76 25.08

e.1)

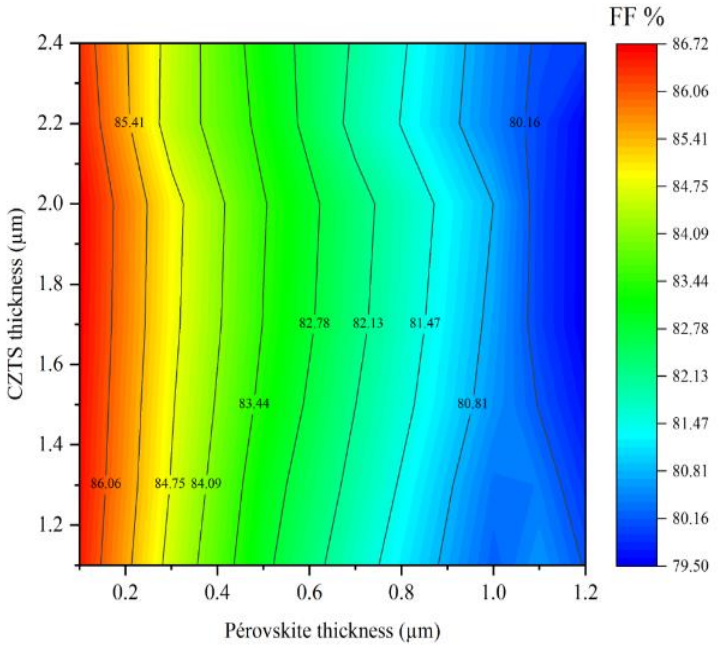
FF %
CZTS thickness (µm)
Pérovskite thickness (µm)
85.41
80.16
82.78
82.13
81.47
83.44
80.81
86.06
84.75
84.09

f.1)

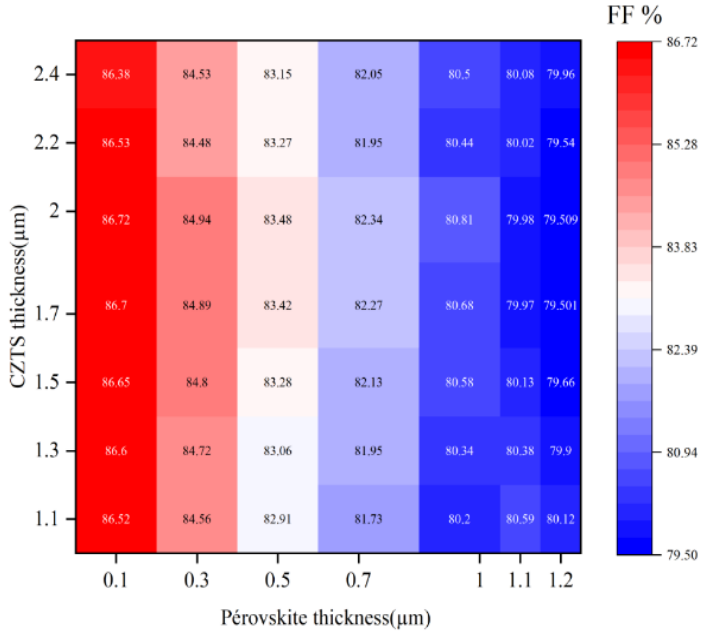
FF %
CZTS thickness(µm)
Pérovskite thickness(µm)
86.38 84.53 83.15 82.05 80.5 80.08 79.96
86.53 84.48 83.27 81.95 80.44 80.02 79.54
86.72 84.94 83.48 82.34 80.81 79.98 79.509
86.7 84.89 83.42 82.27 80.68 79.97 79.501
86.65 84.8 83.28 82.13 80.58 80.13 79.66
86.6 84.72 83.06 81.95 80.34 80.38 79.9
86.52 84.56 82.91 81.73 80.2 80.59 80.12

g.1) h.1)

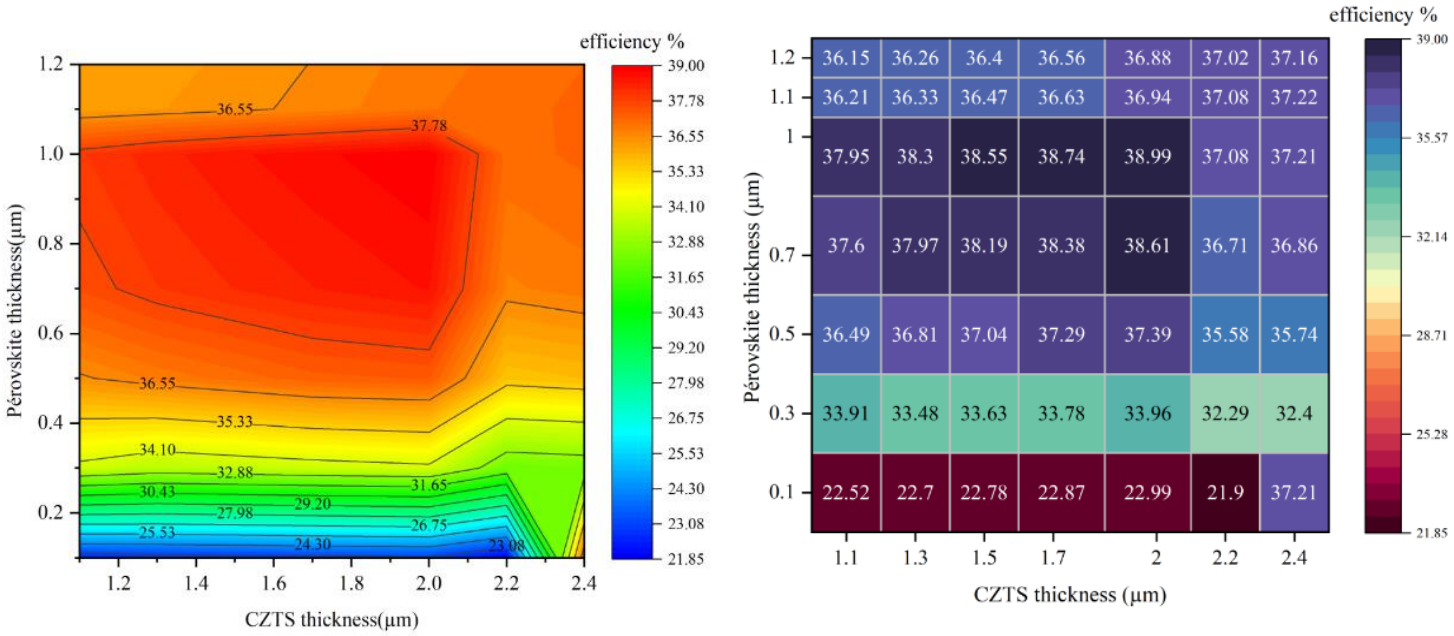

Figure III.10. Effect of thickness on tandem solar cell in different parameters

By progressively increasing the thickness of both the copper zinc tin sulfide (CZTS) and perovskite layers within the tandem solar cell, we observe an initial rise in the short-circuit current (Jsc), as visually represented by the varying colors in the contour profile figure. The gradient from red to blue indicates improved to diminished performance, respectively. The rationale behind this trend lies in the thicker CZTS and perovskite layers enabling enhanced absorption of a wider range of photon energies. Consequently, a higher number of electron-hole pairs are generated, leading to an increase in Jsc. However, it is imperative to exercise caution and consider the open-circuit voltage (Voc), fill factor (FF), and overall efficiency of the tandem solar cell. Each of these characteristics exhibits an optimal range. The contour lines in the figure demonstrate that thicker perovskite (1 µm) and CZTS (1.1 µm) layers can lead to increased recombination rates among charge carriers, resulting in a reduction in photocurrent and a decrease in FF, as depicted in figure III.9 e.1. This observation is corroborated by the heat map displayed in figureIII.9 f.1, which highlights a decline in performance when the perovskite layer thickness is 0.1 µm and the CZTS layer thickness ranges from 1.1 µm to 2.4 µm.

To maximize the efficiency of the tandem solar cell, meticulous consideration must be given to carefully balancing the thicknesses of the CZTS and perovskite layers, as exemplified

in figure g.1 (2 µm CZTS/1 µm perovskite). This ensures optimal overall performance of the tandem solar cell by striking a harmonious equilibrium between light absorption, charge carrier generation, and recombination avoidance.

III.3.2. Effect of CZTS band gap with perovskite (tandem solar cell)

a)

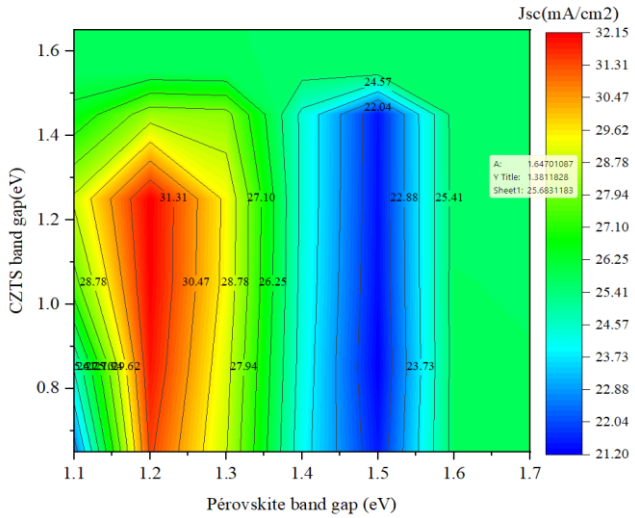

b)

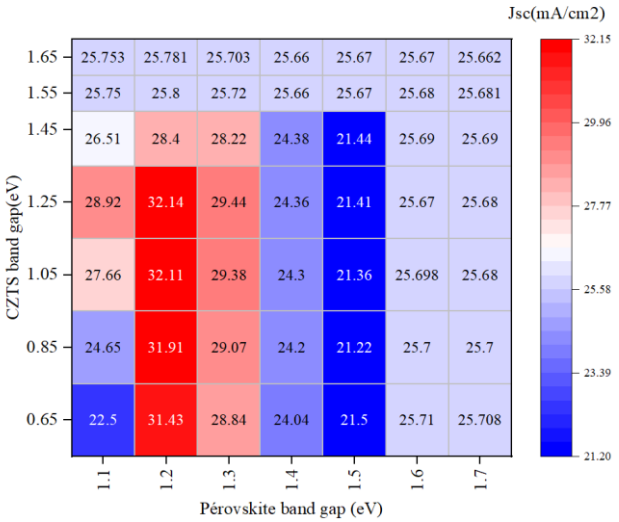

c)

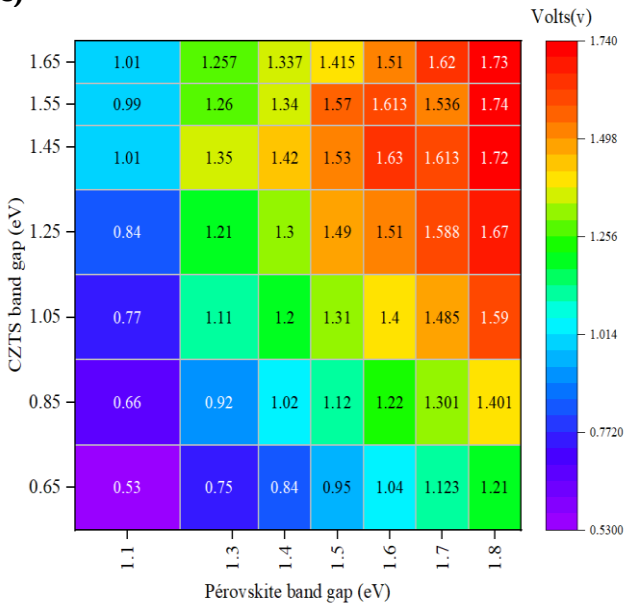

d)

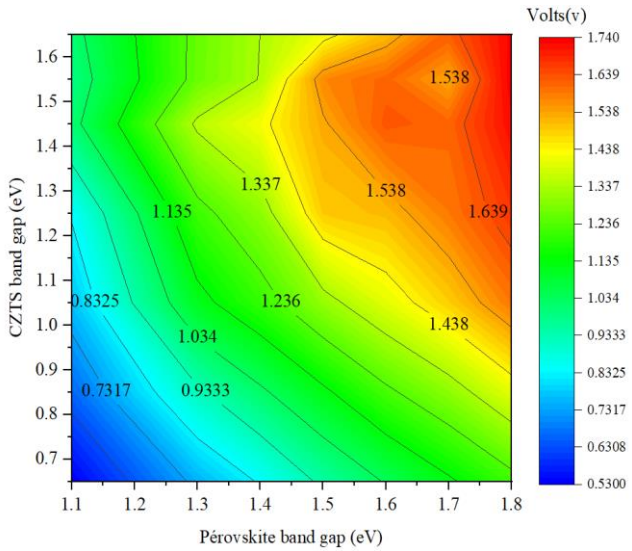

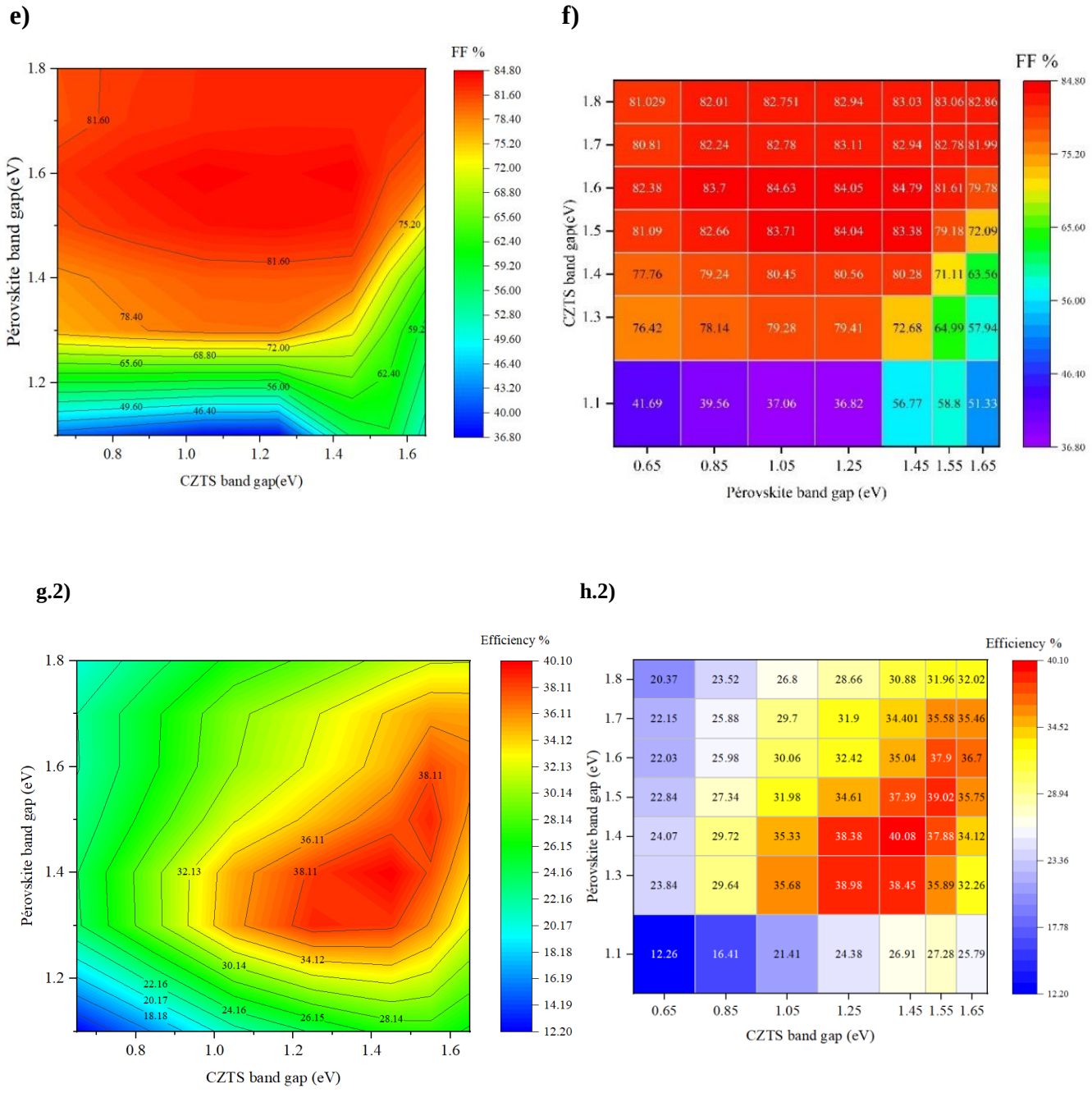

Figure III.11. Effect of band gap on tandem solar cell in different parameters

The band gap plays a crucial role in determining the performance of tandem solar cells. A narrower band gap of 1.2 eV in the perovskite layer facilitates better absorption of shorter wavelengths, resulting in increased photocurrent generation. On the other hand, an optimized band gap of 1.25 eV in the CZTS layer allows for the absorption of longer wavelengths, leading to a higher short-circuit current (Jsc) in the tandem configuration, as depicted in figures a.2 and

b.2. However, when it comes to the open-circuit voltage (Voc), a wider band gap typically results in a higher Voc. This is because a wider band gap enables a larger built-in potential and reduces recombination, ultimately leading to a higher Voc. This relationship between band gap and Voc has been confirmed by the heat map analysis of a tandem solar cell configuration using CZTS with a band gap of 1.65 eV and perovskite with a band gap of 1.25 eV.

To achieve optimal performance in the tandem solar cell structure, it is desirable to have an optimal band gap between the CZTS sub-cell with a band gap of 1.2 eV and the perovskite sub-cell with a band gap of 1.5 eV, as depicted in the aforementioned figure. This optimal band gap helps minimize losses caused by recombination and facilitates efficient charge collection. As a result, the tandem structure can achieve a higher fill factor (FF), which is a measure of how effectively the device converts light into electricity.

To further enhance the overall efficiency of the tandem solar cell, it is essential to balance and maximize the absorption of photons and the generation of photocurrent. By carefully optimize these factors, the tandem solar cell can achieve higher efficiency.

III.4. Tandem solar cell

From our analysis, we conducted a systematic exploration by varying the parameters of the bottom layer, including thickness, band gap, and doping concentration, consisting of CZTS and Si in the tandem solar cell. Our investigation aimed to identify the optimal configuration that would maximize performance.

Through meticulous experimentation and rigorous analysis, we have successfully determined the most favorable combination that the bottom layer can achieve. By carefully adjusting the parameters of CZTS/Si, we have obtained remarkable results in terms of solar cell efficiency.

Furthermore, to further enhance the performance, we integrated a high-efficiency perovskite material, $CsPbI_2Br$, into the tandem structure. This integration has proved highly effective, resulting in an exceptional overall efficiency of nearly 40%.

These findings underscore the significant potential of combining optimized CZTS/Si bottom layers with high-performance perovskite materials in tandem solar cells. The synergistic

effect of these optimized parameters and materials has yielded a substantial enhancement in solar cell efficiency, opening up new possibilities for the development of highly efficient and sustainable energy generation technologies. The table below presents the results obtained from our experimentation.

Table III.4. Output parametric for each structure

	Voc (v)	Jsc (mA/cm^2)	FF %	Efficiency %
Bottom layer cell	0.9041	28.854	85.18	22.22
Top layer Cell	0.8888	27.453	78.18	19.08
Tandem	1.571	25.773	80.08	40.51

I-V characteristic of the optimized tandem solar cell is presented in the figure below

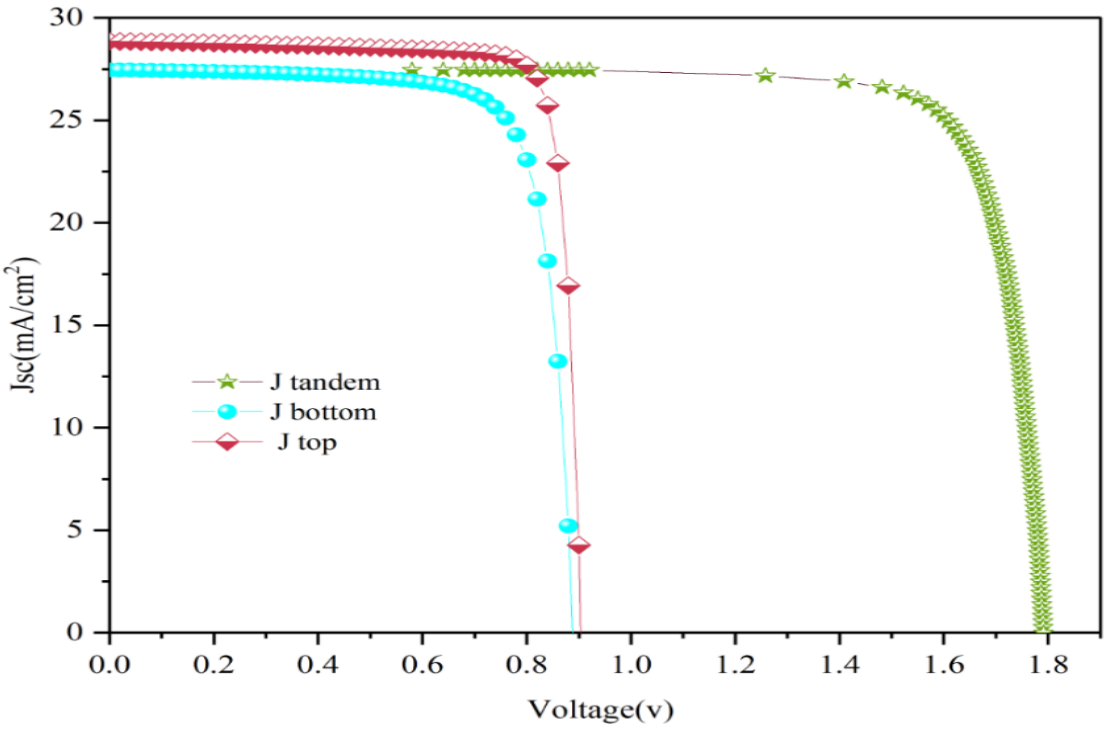

Figure III.12. Characteristic I-V for tandem solar cell

The graph shows three curves: bottom layer I-V, top layer I-V, and tandem layer I-V. These curves represent the electrical behavior of each layer in the tandem solar cell. The bottom layer I-V curve reveals the performance of the bottom layer (CZTS/Si) in response to varying voltage levels. The top layer I-V curve illustrates the electrical behavior of the top layer (CsPbI2Br). The tandem layer I-V curve represents the overall performance of the tandem solar cell.

By analyzing these curves, we can understand the individual contributions of the layers and assess the efficiency and power output of the tandem solar cell. This information helps optimize the design and parameters of each layer for improved performance and higher energy conversion efficiency.

III.5. Conclusion

In the concluding section of this chapter, an in-depth investigation was conducted to study the structural aspects of the bottom cell layer in the tandem solar cell. Through a series of carefully designed experiments, the parameters pertaining to CZTS (thickness, band gap, doping) were systematically varied while keeping all other factors at a fixed state. This rigorous exploration aimed to identify the most optimal configuration that would yield the highest performance and efficiency in the tandem solar cell.

Simultaneously, the parameters of the CdS layer (thickness, band gap, doping) were also subjected to variation, maintaining the remaining layers in a consistent state. This meticulous approach allowed for a comprehensive analysis of the CdS layer's behavior and its impact on the overall performance of the tandem solar cell.

The resulting data was then meticulously analyzed, employing advanced visualization techniques such as contour profiles and heat maps. These graphical representations provided valuable insights into the intricate interplay between different parameters and their influence on the performance characteristics of both the CZTS and perovskite layers.

By integrating and synthesizing the wealth of information gathered from these experiments, a holistic understanding of the optimal parameters for the tandem solar cell was attained. The culmination of this extensive research effort led to the identification of the precise combination of thickness, band gap, and doping concentration that would yield the highest efficiency and performance in the tandem structure.

It is imperative to emphasize that these findings serve as a pivotal stepping stone in the advancement and optimization of tandem solar cell technology. The in-depth exploration of the bottom cell layer, the thorough examination of its various parameters, and the meticulous analysis of the obtained data lay the groundwork for further advancements and breakthroughs in the realm of renewable energy generation.

In essence, this chapter has significantly contributed to the scientific understanding of the structural nuances of the bottom cell layer in tandem solar cells. The robust experimentation, coupled with the visualization techniques employed, has shed light on the optimal configuration

that would unlock the true potential of tandem solar cells, propelling us towards a greener and more sustainable future.

GENERAL CONCLUSION

General conclusion

In this research project, a thorough investigation was conducted, and a tandem solar cell was simulated using the SCAPS numerical simulation software. The tandem cell configuration comprised a top and a bottom solar cell. The bottom solar cell, consisting of Al-ZnO/I-ZnO/n-CdS/p-CZTS/p-Si, underwent meticulous variations in terms of thickness, band gap, and doping in order to optimize its performance. After extensive experimentation, remarkable outcomes were achieved, with the following optimal parameters being discovered: an open-circuit voltage (Voc) of 0.888 V, a short-circuit current density (Jcs) of 28.57 mA/cm², a fill factor (FF) of 85.18%, and an overall efficiency (η) of 22.22%.

Subsequently, the optimized bottom solar cell was combined with a top solar cell configuration consisting of TIO2/Perovskite/CuO2, utilizing parameters obtained from previous studies. The parameters of the top solar cell indicated an open-circuit voltage (Voc) of 0.9021 V, a short-circuit current density (Jsc) of 27.546 mA/cm², a fill factor (FF) of 78.78%, and an efficiency (η) of 19.18%. Remarkably, when the two solar cells were combined, a significantly higher efficiency of over 40% was achieved, accompanied by a fill factor (FF) of approximately 81%.

These findings underscore the potential for enhanced performance in tandem solar cells by optimizing parameters and combining different cell configurations.

Bibliography

[1] Zouhair El Joua, “Réalisation et caractérisation des cellules photovoltaïques organiques ».”

[2] M me BENSMAIN Asmaa, “« investigation de l’ingénierie de bandes des cellules solaires à hétérojonction a-Si:H/cSi : Modélisation et simulation numérique.”

[3] B. M. [1], “Etude Théorique des Cellules Solaires à base de Pérovskite’.”

[4] “Figure (2.1) : Normes de mesures du spectre d’énergie lumineuse émis...,” *ResearchGate*. https://www.researchgate.net/figure/Figure-21-Normes-de-mesures-du-spectre-denergie-lumineuse-emis-par-le-soleil_fig1_339974502 (accessed Jun. 03, 2023).

[5] Mekemeche Abdelkader, “Modélisation à deux dimensions des propriétés physiques de cellules solaires au silicium à base de substrat de type n. Étude de quelques cas particuliers de cellules innovantes.”

[6]] Mahfoud, Abdrrezek., . “Modélisation des cellules solaires tandem à couches minces et à haut rendement.”

[7] Stéphane Vighetti, “Systèmes photovoltaïques raccordés au réseau : Choix et dimensionnement des étages de conversion.”

[8] smaa MOHAMMED KRARROUBI, “Traitement de l’interface anode/matériau organique pour améliorer le rendement des cellules solaires.”

[9] YoussefJouane, “Apportdescouchesinterfacialesàbased’oxydedeZincdéposéparpulvérisationdanslesperformancesdescellulesphotovoltaïquesorganiquescompatiblesavecdessub stratsflexibles.”

[10] Thomas Mambrini, “Caractérisation de panneaux solaires photovoltaïques en conditions réelles d’implantation et en fonction des différentes technologies.”

[11] Dariga Meekhun, “Réalisation d’un système de conversion et de gestion de l’énergie d’un système».”

[12] “http://staff.univ-batna2.dz/sites/default/files/azzoui_boubaker/files/chapitre-.”

[13] “Cellule au silicium monocristallin — Solarpedia.” http://fr.solarpedia.net/wiki/index.php?title=Cellule_au_silicium_monocristallin (accessed Jun. 03, 2023).

[14] J.-C. Muller, “Techniques de l’Ingénieur.”

[15] NAIM Houcine, “Etude de gestion d’une mini-centrale solaire et mise au point d’un dispositif automatique de mesures, contrôles et régulation de l’énergie électrique,”

[16] “https://www.researchgate.net/figure/Cellule-en-silicium-”.

[17] Mohammed Makha, ““Utilisation de diverses électrodes conductrices et transparentes comme anode des cellules photovoltaïques organiques, optimisation del’interface à l’aide des couches tampons.”

[18] “https://www.futura-sciences.com/planete/dossiers/developpement-durable-cellules-photovoltaiques-coeur-panneaux-solaires-1688/page/11/”.

[19] “Cellule au tellurure de cadmium — Solarpedia.” http://fr.solarpedia.net/wiki/index.php?title=Cellule_au_tellurure_de_cadmium (accessed Jun. 03, 2023).

[20] BENNAOUM Menouer, “Etude Théorique des Cellules Solaires à base de Pérovskite’, UNIVERSITE DJILLALI LIABES FACULTE DE GENIE ELECTRIQUE SIDI BEL ABBES.”

[21] K. I. of Technology, “Why perovskite solar cells are so efficient.” https://phys.org/news/2018-04-perovskite-solar-cells-efficient.html (accessed Jun. 03, 2023).
[22] “Pérovskites : leur structure pourrait révolutionner les cellules photovoltaïques.” https://trustmyscience.com/structure-perovskites-pourrait-revolutionner-cellules-photovoltaiques/ (accessed Jun. 03, 2023).
[23] G. M. &HAMDOUNI B. [35], “Etude et Simulation D’une Cellule Photovoltaïque à Pérovskite.”
[24] [36] ZOUARI AHMED Mammar & SLIMANI Abdelhamid, MASTER ACADEMIQUE, “« Simulation Et Optimisation D’une Cellule Solaire A Base Du Pérovskite CH3NH3SnI3 En Architecture NIP.”
[25] S. N. R. N. [28], “NUMERICAL SIMULATION AND PERFORMANCE OPTIMIZATION OF PEROVSKITE SOLAR CELL,” ”. University Of Missouri-Kansas City, 2017.
[26] P. D. [30], “Cellules Solaires à base de Matériaux Pérovskites : De la caractérisation des matériaux à l’amélioration des rendements et de la stabilité. Génie des procédés.,” 2019. Français. NNT : 2019GREAI093. tel- 02499789.
[27] Dylan AMELOT, “Thèse de Doctorat de Sorbonne Université, Etudes des propriétés d’interfaces pour les cellules solaires de nouvelle génération.”
[28] Florian BERRY, “THESE de DOCTORAT DE L’UNIVERSITE DE LYON Opérée au sein de l’Ecole centrale de Lyon, ‘Nanostructuration et cristaux photoniques à base de pérovskites hybrides pour applications photovoltaïques.’”
[29] “(a) Lattice structure of undoped CsPbI2Br supercell, (b), (c) local...,” *ResearchGate*. https://www.researchgate.net/figure/a-Lattice-structure-of-undoped-CsPbI2Br-supercell-b-c-local-structures-of-PbI4Br2_fig1_359926565 (accessed Jun. 05, 2023).
[30] Shen Wang, “Function of Hole Transport Layer Componentsin Perovskite Solar Cells,A dissertation submitted in partial satisfaction of therequirements for the degree Doctor of Philosophy in NanoEngineering 2018,” UNIVERSITY OF CALIFORNIA SANDIEGO.
[31] S. Li, Y.-L. Cao, W.-H. Li, and Z.-S. Bo, “A brief review of hole transporting materials commonly used in perovskite solar cells,” *Rare Met.*, vol. 40, no. 10, pp. 2712–2729, Oct. 2021, doi: 10.1007/s12598-020-01691-z.
[32] P. M. Tembo and V. Subramanian, “Current trends in silicon-based photovoltaic recycling: A technology, assessment, and policy review,” *Solar Energy*, vol. 259, pp. 137–150, Jul. 2023, doi: 10.1016/j.solener.2023.05.009.
[33] H. S. Nugroho *et al.*, “A progress review on the modification of CZTS(e)-based thin-film solar cells,” *Journal of Industrial and Engineering Chemistry*, vol. 105, pp. 83–110, Jan. 2022, doi: 10.1016/j.jiec.2021.09.010.
[34] P. Prabeesh, I. Packia Selvam, and S. N. Potty, “CZTS films from three different routes: crystallite size-dependent properties,” *Mater. Res. Express*, vol. 6, no. 6, p. 065509, Mar. 2019, doi: 10.1088/2053-1591/ab08d5.
[35] H. Katagiri, “Cu2ZnSnS4 thin film solar cells,” *Thin Solid Films*, vol. 480–481, pp. 426–432, Jun. 2005, doi: 10.1016/j.tsf.2004.11.024.
[36] “ResearchGate.” https://www.researchgate.net/figure/Kesterite-stannite-and-PMCA-structures-for-CZTS-CZTSe-structures-are-obtained-by_fig1_234024221/download (accessed Jun. 06, 2023).

[37] R. R. Schnepf *et al.*, “Utilizing Site Disorder in the Development of New Energy-Relevant Semiconductors,” *ACS Energy Lett.*, vol. 5, no. 6, pp. 2027–2041, Jun. 2020, doi: 10.1021/acsenergylett.0c00576.

[38] M. S. Rahman, S. Islam, A. Khandaker, T. Hossain, and M. J. Rashid, “Bilayer CZTS/Si absorber for obtaining highly efficient CZTS solar cell,” *Solar Energy*, vol. 230, pp. 1189–1198, Dec. 2021, doi: 10.1016/j.solener.2021.11.021.

[39] C. Pinzón *et al.*, “Optimization of Inverted All-Inorganic CsPbI3 and CsPbI2Br Perovskite Solar Cells by SCAPS-1D Simulation,” *Solar*, vol. 2, no. 4, Art. no. 4, Dec. 2022, doi: 10.3390/solar2040033.

[40] “What is heat map (heatmap)? | Definition from TechTarget,” *Business Analytics*. https://www.techtarget.com/searchbusinessanalytics/definition/heat-map (accessed Jun. 02, 2023).

[41] “1.3.3.10. Contour Plot.” https://www.itl.nist.gov/div898/handbook/eda/section3/contour.htm (accessed Jun. 03, 2023).

[42] Naceur Selmane, Ali Cheknane &Hikmat S. Hilal,’’ Optimization of Al-Doped ZnO Transparent Conducting Oxide and Emitter Layers for Enhanced Performance of Si Heterojunction Solar Cells, 1.—Laboratoire des semiconducteurs et mate´riaux fonctionnels, Universite´ Amar Telidji de Laghouat, Bd des Martyrs BP37G, Laghouat 03000, Alge´rie. 2.—SSERL, Department of Chemistry, An-Najah National University, Nablus, Palestine.

[43] Naceur Selmane, Ali Cheknane &Hikmat S. Hilal,’’ Optimizing Optical and Electrical Properties of Porous Silicon by Enhancing Morphology through Substrate Type and Electro-Etching Control.

[44] Naceur Selmane, Ali Cheknane &Hikmat S. Hilal,’’ Effect of ZnO-Based TCO on the Performance of a-Si H(n)/a-Si H(i)/c-Si H(p)/Al BSF(p+)/Al Heterojunction Solar Cells

Abstract

This project focuses on simulating and optimizing a tandem photovoltaic solar cell using the one-dimensional simulation tool SCAPS. The primary objective is to enhance the performance of the solar cell by determining optimal parameters such as the thickness, band gap, and doping concentration for the bottom layer based on CZTS/SI. The findings indicate that by fine-tuning specific layer parameters, notable enhancements in electrical performance were achieved. The optimized configuration resulted in remarkable improvements across key metrics, including a high fill factor (FF) of 85.18% and an impressive overall efficiency of 22 %. These outcomes highlight the significant impact of optimizing layer parameters on the performance of the system. furthermore, a top layer perovskite solar cell (CsPbI2br) was integrated into the system based on prior studies. The initial parameters for this layer included a fill factor of 78 % and an overall efficiency over 19 %. To further optimize the tandem structure, variations were introduced in the thickness and band gap. Remarkably, the best results achieved with these modifications were an increased fill factor of 80 % and an improved overall efficiency over 40%. This demonstrates the significant impact of adjusting the layer characteristics on the overall performance of the solar cell system.

Keywords : Solar cells, Perovskite, Simulation, SCAPS, CZTS/SI.

Résume

Ce projet se concentre sur la simulation et l'optimisation d'une cellule solaire photovoltaïque tandem en utilisant l'outil de simulation unidimensionnelle SCAPS. L'objectif principal est d'améliorer les performances de la cellule solaire en déterminant les paramètres optimaux tels que l'épaisseur, la bande interdite et la concentration de dopage pour la couche inférieure basée sur CZTS/SI. Les résultats indiquent que grâce à l'ajustement fin des paramètres spécifiques de la couche, des améliorations notables des performances électriques ont été obtenues. La configuration optimisée a conduit à des améliorations remarquables sur des critères clés, notamment un facteur de remplissage élevé (FF) de 85,18 % et une efficacité globale impressionnante de 22 %. Ces résultats mettent en évidence l'impact significatif de l'optimisation des paramètres de la couche sur les performances du système. De plus, une couche supérieure de cellule solaire en pérovskite (CsPbI2br) a été intégrée dans le système sur la base

d'études antérieures. Les paramètres initiaux de cette couche comprenaient un facteur de remplissage de 78 % et une efficacité globale de plus de 19 %. Pour optimiser davantage la structure tandem, des variations ont été introduites dans l'épaisseur et la bande interdite. De manière remarquable, les meilleurs résultats obtenus avec ces modifications étaient un facteur de remplissage augmenté de 80 % et une efficacité globale améliorée de plus de 40 %. Cela démontre l'impact significatif de l'ajustement des caractéristiques de la couche sur les performances globales du système de cellules solaires

Mots clés : Cellules solaires, Pérovskite, Simulation, SCAPS, CZTS/SI.

ملخص

يتركز هذا المشروع على محاكاة وتحسين خلية شمسية فوتوفولتائية ثنائية باستخدام أداة المحاكاة ثنائية الأبعاد SCAPS. الهدف الرئيسي هو تحسين أداء الخلية الشمسية عن طريق تحديد المعلمات المثلى مثل السمك وفجوة النطاق وتركيز الشوائب للطبقة السفلية المستندة على CZTS/SI. تشير النتائج إلى أنه من خلال ضبط المعلمات المحددة للطبقة، تم تحقيق تحسينات ملحوظة في الأداء الكهربائي. أدى التكوين المحسن إلى تحسينات ملحوظة في المعايير الرئيسية، بما في ذلك نسبة التعبئة العالية (FF) بنسبة 85.18٪ وكفاءة عامة مثيرة للإعجاب بنسبة 22٪. تسلط هذه النتائج الضوء على أهمية ضبط معلمات الطبقة على أداء النظام. بالإضافة إلى ذلك، تم دمج طبقة علوية لخلية شمسية بيروفسكيت (CsPbI2br) في النظام بناءً على الدراسات السابقة. المعلمات الأولية لهذه الطبقة تشمل نسبة التعبئة بنسبة 78٪ وكفاءة عامة تزيد عن 19٪. لتحسين الهيكل المتكامل بشكل أكبر، تم إدخال تغييرات في السمك وفجوة النطاق. بشكل مذهل، تم تحقيق أفضل النتائج مع هذه التعديلات، وهي زيادة في نسبة التعبئة بنسبة 80٪ وتحسين في الكفاءة العامة تفوق 40٪. يوضح ذلك الأثر الكبير لضبط خصائص الطبقة على الأداء العام لنظام الخلية الشمسية.

الكلمات الرئيسية: خلايا شمسية، بيروفسكيت، محاكاة، SCAPS، CZTS/SI